Inorganic Chemistry, Vol. 17, No. 2, 1978 **457**

Contribution from the School of Chemical Sciences,
University of Illinois, Urbana, Illinois 61801

Magnetic Exchange Interactions in Transition-Metal Dimers. 13. Structural Characterization of the Two Hydrogen-Bonded Mn(II) Dimers $[Mn_2(tren)_2(NCS)_2](BPh_4)_2$ and $[Mn_2(tren)_2(NCO)_2](BPh_4)_2$. A Series of Outer-Sphere Manganese Dimers Formed from Trigonal-Bipyramidal Mn(II) Complexes[1]

EDWARD J. LASKOWSKI and DAVID N. HENDRICKSON*[2]

Received July 13, 1977

The structures of $[Mn_2(tren)_2(NCO)_2](BPh_4)_2$ and $[Mn_2(tren)_2(NCS)_2](BPh_4)_2$, where tren is 2,2′,2″-triaminotriethylamine, have been determined using heavy-atom, least-squares refinement methods in conjunction with data measured on a four-circle x-ray diffractometer. Both compounds crystallize in the monoclinic space group $P2_1/c$ with two formula weights per unit cell. Measurements on the cyanate compound give a = 14.167 (7) Å, b = 10.753 (8) Å, c = 19.654 (11) Å, β = 96.62 (3)°, d(calcd) = 1.25, and d(exptl) = 1.25 (2) g cm^{-3}, whereas, in the case of the thiocyanate compound, a = 14.882 (6) Å, b = 9.843 (4) Å, c = 21.109 (6) Å, β = 98.04 (3)°, d(calcd) = 1.26, and d(exptl) = 1.26 (2) g cm^{-3}. The cyanate compound was refined to conventional discrepancy factors of R_F = 0.071 and R_{wF} = 0.058 for 2938 observed ($F_o \geq 2\sigma$) reflections. The thiocyanate compound was refined to R_F = 0.051 and R_{wF} = 0.070 for 2777 observed ($F_o \geq 2\sigma$) reflections. Both compounds are composed of BPh_4^- anions and discrete outer-sphere-bridged $[Mn_2(tren)_2(X)_2]^{2+}$ cations (X^- = NCO^- or NCS^-). The outer-sphere association consists of hydrogen-bonding contacts between two distorted trigonal-bipyramidal $[Mn(tren)(X)]^+$ units. Each X^- binds with its nitrogen atom to one manganese ion and is involved in hydrogen-bonding contacts with two tren nitrogen atoms from the coordination sphere of the second manganese ion. The preparation of the analogous Cl^-, Br^-, and CN^- compounds is reported. From IR work, it is concluded that the corresponding N_3^- compound has six-coordinate manganese ions. Variable-temperature (4.2–296 K) magnetic susceptibility and EPR results are presented for several of the outer-sphere-associated compounds and compared with results obtained for similar monomeric species. Doping Mn^{2+} into [Zn(Me$_6$tren)I]I gives a sample that, from X- and Q-band EPR spectra, is found to have an axial zero-field splitting parameter (D in DS_z^2) of 0.20 cm^{-1}. This relatively large zero-field interaction is a consequence of the five-coordinate trigonal-bipyramidal coordination geometry. Analysis of the susceptibility data for $[Mn_2(tren)_2(NCO)_2](BPh_4)_2$ with a monomer $S = {}^5/_2$ model gives unreasonable parameters, whereas an isotropic exchange interaction ($S_1 = S_2 = {}^5/_2$) model gives reasonable values of J = −0.15 cm^{-1} and D = −0.29 cm^{-1} with the assumption that g is isotropic and equal to 2.0. A similar-magnitude antiferromagnetic exchange interaction is found for the thiocyanate compound, whereas the interaction in the cyanide compound is negligible. Complicated EPR spectra showing signals over very extended magnetic field ranges are seen for powdered samples of these Mn(II) outer-sphere dimers. Frozen-glass and single-crystal EPR results are presented in an effort to understand the complicated spectra.

Introduction

In previous papers[3-5] in this series, structural, magnetic, and EPR results were presented for a series of outer-sphere Cu(II) dimers, $[Cu_2(tren)_2(X)_2](BPh_4)_2$, where X^- is Br^-, Cl^-, CN^-, OH^-, NCO^-, and NCS^- and tren is 2,2′,2″-triaminotriethylamine. The $[Cu_2(tren)_2(X)_2]^{2+}$ ions are dimeric by virtue of the X^- group bonded to one copper ion participating in hydrogen bonding to primary amines of the tren moiety ligated to the second copper ion. The hydrogen bonds in these outer-sphere dimers propagate magnetic exchange interactions with J in the range of −3.5 to −0.05 cm^{-1}.

In this paper, the results of magnetic susceptibility and EPR studies are reported for the series $[Mn_2(tren)_2(X)_2](BPh_4)_2$, where X^- is variously Br^-, Cl^-, CN^-, N_3^-, NCO^-, or NCS^-. Single-crystal structures have been reported for only a few five-coordinate Mn(II) compounds.[6-10] The compound [Mn(Me$_6$tren)Br]Br, where Me$_6$tren is the *N*-hexamethylated analogue of tren, is known[11] to consist of *monomeric* trigonal-bipyramidal cations. Only one dimeric five-coordinate Mn(II) compound has been characterized crystallographically, bis(2,2′-biquinolyl)-di-μ-chloro-dimanganese(II).[12] The paucity of structurally characterized five-coordinate Mn(II) species and a need to know whether the $[Mn_2(tren)_2(X)_2](BPh_4)_2$ compounds consist of outer-sphere Mn(II) dimers led to the determination of the structures of the cyanate and thiocyanate compounds; the results of these two structure determinations and of detailed magnetism and EPR studies are reported herein.

Experimental Section

Compound Preparation. Initial attempts to prepare $[Mn_2(tren)_2(X)_2](BPh_4)_2$, where X^- = NCO^-, NCS^-, N_3^-, CN^-, Cl^-, or Br^-, first in the open air and then in a glovebag, resulted in products which were slightly decomposed. These compounds are air sensitive while wet, changing in color from white to tannish brown within seconds of their formation, but are stable indefinitely when dry. The procedure and apparatus described below provide a convenient method for synthesizing these compounds and handling them until they are dry. The apparatus, pictured in Figure 1, consists of three flasks connected by two Schlenk tubes, allowing two filtrations. The apparatus is wired together, for two inversions of the apparatus are required and this serves to simplify the manipulation of the apparatus.

A solution of 1.69 g (10 mmol) of $MnSO_4 \cdot 6H_2O$ in 25 mL of water was placed in flask A. Solutions of 1.5 mL of tren (Ames Laboratories, Inc.) in 25 mL of water, 10 mmol of the sodium salt of the bridging anion X^- in 25 mL of water, and 0.25 g of $NaBPh_4$ in 25 mL of water were placed in each of three flasks which were external to the apparatus and were sealed with septum caps. Nitrogen gas was bubbled through all of these solutions via a system of flexible "pipes" which also served as a means for transferring a solution into flask A. The pipes were made of polypropylene tubing fitted at each end with 17 gauge syringe needles. A stirring bar was placed in flask A. After approximately 3 h of bubbling nitrogen gas through all four solutions, the tren solution and then the solution containing X^- were transferred to A. The transfer was aided by applying a vacuum at stopcock E. The apparatus was then inverted to filter the solution (Mn^{2+} + tren + X^-) through frit D. Nitrogen gas pressure was applied at C and a vacuum at E to aid in the filtration. After several milliliters of filtered solution was accumulated in flask G, the $NaBPh_4$ solution was introduced through the septum cap on outlet F. Best results were obtained when the BPh_4^- solution entered below the solution level, thus minimizing the area of contact between reactive solution and the atmosphere. A white precipitate formed immediately. When all solutions were combined in flask G, the apparatus was again inverted to filter the product. Nitrogen gas pressure was applied at E and a vacuum at L. Valve H was closed when the filtration was complete, and the right-hand

0020-1669/78/1317-0457$01.00/0

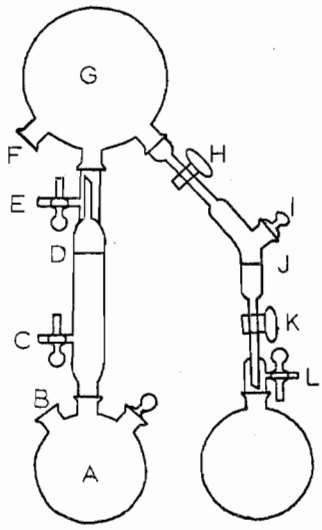

Figure 1. Schematic drawing of the apparatus used to make the compounds.

side of the apparatus was removed from flask G. The Schlenk tube was then fitted with an adaptor so that the product on frit J could be washed with degassed water when stopcock H was opened. After the product was washed, stopcocks H and K were closed and the Schlenk tube was transferred to a vacuum line to pump off any remaining water. When dry, the product was removed through opening I in the side of the Schlenk tube. Analytical data for these compounds are given in Table I.[13]

Crystals of these compounds can be grown by slow evaporation of a degassed acetonitrile solution in a drybox. The crystalline samples are clear rectangular prisms which may have a slight coloration, ranging from a faint greenish tint in the case of the bromide compound to a slightly brownish tint in the case of the thiocyanate compound.

Physical Measurements. Infrared spectra, EPR spectra, and variable-temperature magnetic susceptibility data were obtained as described in a previous paper.[1]

Crystal Measurements for $[Mn_2(tren)_2(NCO)_2](BPh_4)_2$. Slow evaporation of an acetonitrile solution of the cyanate compound gave clear, colorless crystals in the shape of rectangular prisms. Several crystals were mounted in Lindemann capillary tubes with the needle axis of the crystal aligned parallel to the length of the capillary. Preliminary precession photographs revealed systematic absences for $0k0$, $k = 2n + 1$, and $h0l$, $l = 2n + 1$, which indicated the space group to be the monoclinic system $P2_1/c$ [C_{2h}^5; No. 14]. Diffraction data were collected at the University of Illinois on a computer-controlled Picker FACS-1 diffractometer. The details of the data collection are given in Table II. The unit cell parameters were determined from the least-squares refinement of 13 strong reflections which had been hand centered. Lorentz and polarization corrections were applied to the data. In light of the small variation in the transmission factors (91.7 ± 1.2%), no absorption correction was applied.

Crystal Measurements for $[Mn_2(tren)_2(NCS)_2](BPh_4)_2$. The thiocyanate crystals, also obtained from acetonitrile, were clear, light tan hexagonal prisms. The crystals were glued to a quartz fiber such that the needle axis was perpendicular to the fiber and the axis of the fiber ran through two opposite corners of the crystal. As with the cyanate crystals, these crystals show no signs of decomposition upon prolonged exposure to Mo Kα x radiation. Preliminary precession photographs revealed the approximate unit cell dimensions and indicated systematic absences for $0k0$, $k = 2n + 1$, and $h0l$, $l = 2n + 1$. From this information, the space group was determined to be the monoclinic system $P2_1/c$. Diffraction data were collected by Molecular Structure Corp. employing a Syntex $P\bar{1}$ computer-controlled diffractometer. The crystal was accurately centered using the x and y coordinates of 15 reflections and an autoindexing program for selection of the best unit cell. The details of the data collection are given in Table III. The cell constants were obtained from a least-squares refinement of the setting angles for 15 strong reflections. Lorentz and polarization corrections were applied to the data. In light of the small variation in the transmission factors (83.0 ± 1.8%), no absorption correction was applied.

Table II. Experimental Data for the X-Ray Diffraction Study of $[Mn_2(tren)_2(NCO)_2](BPh_4)_2$

Crystal Parameters

a = 14.167 (7) Å	Space group $P2_1/c$
b = 10.753 (8) Å	Z = 2 dimers
c = 19.654 (11) Å	Mol wt 1124.82
β = 96.62 (3)°	ρ(calcd) = 1.25 g cm^{-3}
V = 2974 (2) Å^3	ρ(obsd) = 1.25 (2) g cm^{-3} (flotation in toluene–bromotoluene)

Measurement of Intensity Data

Radiation: Mo Kα, λ 0.7107 Å
Monochromator: graphite crystal
Attenuators: copper; attenuation factor 3
Takeoff angle: 1°
Crystal orientation: mounted along needle axis
Reflections measured: $h,k,\pm l$
Maximum 2θ: 45°
Scan type: θ–2θ scan technique
Scan speed: 2.0°/min
Scan length: symmetrical scan, 2θ = 1.8°, corrected for Kα_1–Kα_2
Background measurement: stationary crystal, stationary counter; 10 s each at beginning and end of 2θ scan
Standard reflections: three standards, (060), (520), and ($\bar{2}$08) measured after every 50 reflections; no systematic change in intensity during data collection
Reflections collected: 3899 unique reflections; 2938 observed above 2σ cutoff
Temperature: 20 °C

Treatment of Intensity Data

Definition of σ: $\sigma(F_o^2) = (Lp)^{-1}[T_c + 0.25(t_c/t_b)^2(B_1 + B_2) + (0.07I)]^{1/2}$ where T_c is the total count, (t_c/t_b) is the ratio of time counting peak intensity to that counting backgrounds, and B_1 and B_2 are background counts; $\sigma(F_o) = \sigma(F_o^2)/2F_o$
Weighting scheme: $w = 2F_o/\sigma(F_o^2)$
Absorption coefficient: 5.00 cm^{-1}
Range of transmission factors: 90.5–92.8%

Table III. Experimental Data for the X-Ray Diffraction Study of $[Mn_2(tren)_2(NCS)_2](BPh_4)_2$

Crystal Parameters

a = 14.882 (6) Å	Space group $P2_1/c$
b = 9.843 (4) Å	Z = 2 dimers
c = 21.109 (6) Å	Mol wt 1156.98
β = 98.04 (3)°	ρ(calcd) = 1.26 g cm^{-3}
V = 3062 (2) Å^3	ρ(obsd) = 1.26 (2) g cm^{-3} (flotation in toluene–bromotoluene)

Measurement of Intensity Data

Radiation: Mo Kα, λ 0.7107 Å
Monochromator: graphite crystal incident beam
Crystal-to-detector distance: 19 cm
Counter aperature width: 2 mm
Incident beam collimator diameter: 1.5 mm
Takeoff angle: 3°
Crystal orientation: random
Reflections measured: $h,k,\pm l$
Maximum 2θ: 45°
Scan type: θ–2θ scan technique
Scan speed: 3.0–24.0°/min; variable dependent on intensity of reflection
Background measurement: stationary crystal, stationary counter; taken at each end of scan range such that the scan time equaled the background counting time
Standard reflections: three standards measured after every 100 reflections; no systematic change in intensity during data collection
Reflections collected: 4020 unique reflections; 2777 observed above 2σ cutoff
Temperature: 21 °C

Treatment of Intensity Data

Definition of σ: $\sigma(I) = [S^2(C + R^2B) + (0.07I)^2]^{1/2}$ and $\sigma(F_o^2) = [S^2(C + R^2B) + (0.07F_o^2)]^{1/2}$ where S is the scan rate, C is the total integrated peak count, R is the ratio of scan time to background counting time, and B is the total background count
Weighting scheme: $w = 4F_o^2/(\sigma(F_o^2))^2$
Absorption coefficient: 5.48 cm^{-1}
Range of transmission factors: 81.2–84.8%

Table IV. Positional Parameters for All Atoms in $[Mn_2(tren)_2(NCO)_2](BPh_4)_2$ Including Isotropic Thermal Parameters for All Hydrogens[a]

Atom	x	y	z	Atom	x	y	z	B, Å²
Mn	0.15174 (6)	0.09471 (8)	0.10198 (4)	H(1)	0.2637	−0.0302	0.1998	4.90
N(1)	0.2784 (3)	0.2410 (4)	0.1334 (2)	H(2)	0.1679	−0.0067	0.2286	4.90
N(2)	0.2146 (3)	0.0333 (4)	0.2044 (2)	H(3)	0.2366	0.0768	−0.0117	4.80
N(3)	0.2575 (3)	0.0474 (4)	0.0335 (2)	H(4)	0.2623	−0.0426	0.0307	4.80
N(4)	0.0799 (3)	0.2761 (5)	0.0966 (3)	H(5)	0.0531	0.2939	0.1396	5.46
N(5)	0.0356 (3)	−0.0203 (5)	0.0882 (2)	H(6)	0.0271	0.2781	0.0613	5.46
C(1)	0.3276 (4)	0.2026 (5)	0.2008 (3)	H(7)	0.3577	0.2729	0.2244	4.24
C(2)	0.2605 (4)	0.1381 (6)	0.2431 (3)	H(8)	0.3790	0.1444	0.1936	4.24
C(3)	0.3409 (4)	0.2332 (5)	0.0791 (3)	H(9)	0.2100	0.1971	0.2526	5.18
C(4)	0.3516 (4)	0.1018 (6)	0.0561 (3)	H(10)	0.2905	0.1127	0.2872	5.18
C(5)	0.2353 (4)	0.3644 (6)	0.1368 (4)	H(11)	0.4042	0.2669	0.0939	4.31
C(6)	0.1477 (5)	0.3754 (6)	0.0863 (3)	H(12)	0.3171	0.2809	0.0389	4.31
C(7)	−0.0133 (4)	−0.0993 (7)	0.0648 (3)	H(13)	0.3822	0.0530	0.0950	4.86
O	−0.0656 (3)	−0.1800 (5)	0.0406 (2)	H(14)	0.3931	0.0946	0.0208	4.86
B	0.7328 (4)	0.2723 (6)	0.1067 (3)	H(15)	0.2177	0.3806	0.1820	5.03
C(11)	0.7153 (4)	0.1246 (5)	0.1232 (2)	H(16)	0.2789	0.4293	0.1270	5.03
C(12)	0.6245 (4)	0.0747 (6)	0.1206 (3)	H(17)	0.1631	0.3670	0.0403	6.03
C(13)	0.6061 (5)	−0.0510 (7)	0.1246 (3)	H(18)	0.1165	0.4550	0.0893	6.03
C(14)	0.6803 (5)	−0.1336 (6)	0.1342 (3)	H(12b)[b]	0.5695	0.1314	0.1142	4.41
C(15)	0.7722 (5)	−0.0894 (6)	0.1392 (3)	H(13b)	0.5386	−0.0805	0.1193	5.36
C(16)	0.7891 (4)	0.0363 (6)	0.1331 (3)	H(14b)	0.6640	−0.2238	0.1349	4.88
C(21)	0.7357 (4)	0.2733 (5)	0.0225 (3)	H(15b)	0.8258	−0.1505	0.1478	4.88
C(22)	0.6544 (4)	0.2508 (5)	−0.0229 (3)	H(16b)	0.8561	0.0657	0.1368	3.55
C(23)	0.6545 (4)	0.2468 (5)	−0.0935 (3)	H(22b)	0.5939	0.2358	−0.0036	3.97
C(24)	0.7400 (5)	0.2627 (5)	−0.1208 (3)	H(23b)	0.5950	0.2312	−0.1245	4.09
C(25)	0.8213 (4)	0.2827 (5)	−0.0775 (3)	H(24b)	0.7410	0.2579	−0.1709	3.94
C(26)	0.8199 (4)	0.2874 (5)	−0.0077 (3)	H(25b)	0.8811	0.2922	−0.0977	4.19
C(31)	0.6453 (4)	0.3573 (5)	0.1286 (3)	H(26b)	0.8797	0.3021	0.0216	3.72
C(32)	0.6132 (4)	0.3411 (5)	0.1933 (3)	H(32b)	0.6418	0.2735	0.2232	3.96
C(33)	0.5441 (4)	0.4153 (7)	0.2170 (3)	H(33b)	0.5222	0.3993	0.2619	4.84
C(34)	0.5041 (4)	0.5101 (7)	0.1767 (4)	H(34b)	0.4563	0.5634	0.1937	5.38
C(35)	0.5325 (5)	0.5289 (6)	0.1127 (4)	H(35b)	0.5026	0.5958	0.0822	5.58
C(36)	0.6031 (4)	0.4549 (6)	0.0909 (3)	H(36b)	0.6245	0.4716	0.0446	4.56
C(41)	0.8290 (4)	0.3333 (5)	0.1472 (3)	H(42b)	0.8594	0.2012	0.2236	3.39
C(42)	0.8801 (4)	0.2842 (5)	0.2061 (3)	H(43b)	0.9911	0.3025	0.2840	4.64
C(43)	0.9572 (4)	0.3438 (7)	0.2423 (3)	H(44b)	1.0431	0.4990	0.2448	5.33
C(44)	0.9868 (4)	0.4567 (7)	0.2204 (4)	H(45b)	0.9595	0.5952	0.1462	4.98
C(45)	0.9375 (5)	0.5129 (6)	0.1630 (4)	H(46b)	0.8262	0.4915	0.0887	4.33
C(46)	0.8607 (4)	0.4499 (5)	0.1285 (3)					

[a] Estimated standard deviations of the least significant figure are shown in parentheses. [b] A small b designates hydrogens on the tetraphenylborate anion.

Structure Solution and Refinement for $[Mn_2(tren)_2(NCO)_2](BPh_4)_2$. All calculations on this structure were carried out on either an IBM 1800 or an IBM 360/75 computer, both located at the University of Illinois.[14] The Mn, H, N, O, and B atoms were assigned scattering factors given by Hansen,[15] while the C atoms were assigned the scattering factors from Cromer and Mann.[16] The manganese atom was also corrected for anomalous dispersion.[17] Using 2938 observed reflections with $F_o \geq 2\sigma$, a three-dimensional Patterson map was generated. All nonhydrogen atoms were located by means of subsequent Fourier and difference-Fourier maps based upon the metal-atom phasing. After two cycles of refinement of the positional parameters of the nonhydrogen atoms, the isotropic thermal parameters were then allowed to vary. Two additional cycles brought the structure to convergence with $R_F = 0.128$ and $R_{wF} = 0.121$ where

$$R_F = \Sigma(|F_o| - |F_c|)/\Sigma|F_o|$$

$$R_{wF} = (\Sigma w(|F_o| - |F_c|)^2/\Sigma w F_o^2)^{1/2}$$

The function minimized was $\sum w||F_o| - |F_c||^2$. Due to limitations in the number of parameters which could be handled by the least-squares program, each cycle of refinement with anisotropic thermal parameters was done in two parts, first varying the cation position and thermal parameters and then the anion parameters. After two such cycles with all atoms having anisotropic thermal parameters, hydrogen atoms were added to the model. The positions of the hydrogen atoms were calculated assuming C–H and N–H bond distances of 0.95 Å and bond angles for the appropriate hydridizations. The hydrogen atoms were given the isotropic thermal parameters of the atoms to which they were bonded. After several cycles of least-squares refinement (hydrogen atom positional and thermal parameters not refined), the structure determination reached convergence with $R_F = 0.071$ and $R_{wF} = 0.058$. The final "goodness of fit", defined as $[\sum w(|F_o| - |F_c|)^2/(m-n)]^{1/2}$ where m is the number of reflections and n is the number of parameters varied, was 1.54. Examination of the final difference-Fourier map showed no peaks greater than 0.50 e/Å³. Final positional and thermal parameters are given in Tables IV and V. The final values of $|F_o|$ and $|F_c|$ for the 3899 reflections are available in the supplementary material.

Structure Solution and Refinement for $[Mn_2(tren)_2(NCS)_2](BPh_4)_2$. Solution of the structure to convergence with isotropic thermal parameters was carried out by Molecular Structure Corp. In this refinement the atomic scattering factors were taken from ref 18. The solution was obtained by using standard heavy-atom techniques and least-squares refinement. Five rounds of full-matrix least-squares refinement gave $R_F = 0.129$ and $R_{wF} = 0.187$. The manganese and sulfur atoms were then given anisotropic thermal parameters and two further rounds of refinement gave $R_F = 0.097$ and $R_{wF} = 0.141$.

The refinement with anisotropic thermal parameters for all nonhydrogen atoms was completed at the University of Illinois. In this last stage of the refinement, the Mn, N, B, and H atoms were given the spherical-atom scattering factors reported by Hansen,[15] while the C and S atoms were given those reported by Cromer and Mann.[16] Sulfur and manganese atoms were corrected for anomalous dispersion.[17] The parameters obtained from Molecular Structure Corp. were used as starting points for the anisotropic refinement. After two full cycles of refinement, hydrogen atoms were added to the model using positional and thermal parameters obtained as indicated for the NCO^- compound. The R factor converged to its final value after three more cycles of anisotropic refinement. As in the previous structure determination, hydrogen atom parameters were not varied. The final discrepancy factors were $R_F = 0.051$ and $R_{wF} = 0.070$ with a goodness of fit of 1.37. The final difference-Fourier map showed one peak of 0.51 e/Å³ of unknown origin. No other large peaks or valleys were present. The final positional and thermal parameters

Table V. Anisotropic Thermal Parameters for $[Mn_2(tren)_2(NCO)_2](BPh_4)_2 \times 10^4$ [a]

Atom	B_{11}	B_{22}	B_{33}	B_{12}	B_{13}	B_{23}
Mn	47.2 (5)	78.7 (9)	30.7 (3)	−5.0 (7)	4.0 (3)	−9.0 (5)
N(1)	56 (3)	71 (5)	29 (2)	0 (3)	7 (2)	−2 (2)
N(2)	67 (3)	100 (6)	29 (2)	−21 (4)	0 (2)	−1 (2)
N(3)	71 (3)	93 (5)	26 (2)	12 (3)	7 (2)	−3 (2)
N(4)	51 (3)	112 (6)	51 (2)	10 (4)	4 (2)	−8 (3)
N(5)	54 (3)	115 (7)	31 (2)	−12 (4)	0 (2)	0 (3)
C(1)	59 (4)	100 (7)	26 (2)	−21 (4)	−3 (2)	−10 (3)
C(2)	72 (4)	111 (8)	22 (2)	−11 (5)	2 (2)	−1 (3)
C(3)	55 (4)	99 (7)	29 (2)	−21 (4)	7 (2)	5 (3)
C(4)	48 (4)	141 (8)	27 (2)	9 (5)	6 (2)	−11 (4)
C(5)	65 (4)	84 (7)	43 (3)	−8 (5)	5 (3)	−4 (3)
C(6)	97 (5)	74 (8)	52 (3)	28 (6)	5 (3)	5 (4)
C(7)	42 (4)	113 (8)	32 (2)	−4 (5)	11 (2)	−4 (4)
O	77 (3)	164 (7)	67 (2)	−48 (4)	19 (2)	−42 (3)
B	31 (4)	70 (7)	24 (2)	1 (4)	3 (2)	−2 (3)
C(11)	38 (3)	81 (7)	14 (2)	2 (4)	−1 (2)	−1 (3)
C(12)	43 (4)	86 (7)	35 (2)	1 (4)	5 (2)	2 (3)
C(13)	67 (5)	115 (9)	31 (2)	−22 (5)	13 (3)	4 (4)
C(14)	86 (5)	83 (7)	25 (2)	−10 (5)	1 (3)	15 (3)
C(15)	69 (5)	95 (8)	26 (2)	24 (5)	4 (2)	10 (4)
C(16)	45 (4)	85 (7)	21 (2)	2 (4)	6 (2)	1 (3)
C(21)	37 (3)	49 (6)	24 (2)	12 (4)	0 (2)	−1 (3)
C(22)	38 (4)	83 (6)	29 (2)	11 (4)	5 (2)	4 (3)
C(23)	50 (4)	94 (7)	22 (2)	12 (4)	−9 (2)	−3 (3)
C(24)	83 (5)	73 (6)	19 (2)	8 (5)	6 (3)	−4 (3)
C(25)	55 (4)	92 (7)	27 (2)	7 (4)	14 (2)	−1 (3)
C(26)	41 (4)	90 (7)	22 (2)	−1 (4)	0 (2)	2 (3)
C(31)	33 (3)	81 (6)	21 (2)	1 (4)	−2 (2)	−1 (3)
C(32)	45 (4)	94 (7)	21 (2)	6 (4)	3 (2)	0 (3)
C(33)	53 (4)	145 (9)	27 (2)	3 (5)	13 (2)	−14 (4)
C(34)	46 (4)	150 (10)	38 (3)	26 (5)	−4 (3)	−30 (4)
C(35)	68 (5)	115 (8)	37 (3)	29 (5)	2 (3)	−4 (4)
C(36)	53 (4)	93 (7)	25 (2)	17 (4)	9 (2)	−4 (3)
C(41)	33 (3)	69 (6)	22 (2)	10 (4)	5 (2)	0 (3)
C(42)	45 (4)	76 (6)	25 (2)	−2 (4)	5 (2)	−9 (3)
C(43)	51 (4)	128 (8)	27 (2)	11 (5)	−4 (2)	−14 (4)
C(44)	51 (5)	140 (10)	42 (3)	−16 (6)	2 (3)	−37 (4)
C(45)	57 (5)	92 (8)	45 (3)	−20 (5)	16 (3)	−21 (4)
C(46)	59 (4)	68 (7)	30 (2)	−2 (4)	9 (2)	−3 (3)

[a] The form of the anisotropic thermal ellipsoid is given by $B_{11}h^2 + B_{22}k^2 + B_{33}l^2 + 2B_{12}hk + 2B_{13}hl + 2B_{23}kl$. Estimated standard deviations of the least significant figure are given in parentheses.

are given in Tables VI and VII. Final values of $|F_o|$ and $|F_c|$ for the 4020 reflections appear in the supplementary material.

Results and Discussion

Structures of $[Mn_2(tren)_2(NCO)_2](BPh_4)_2$ and $[Mn_2(tren)_2(NCS)_2](BPh_4)_2$. The structures of these two compounds have been determined by single-crystal x-ray diffraction techniques. Discrete cationic $[Mn_2(tren)_2X_2]^{2+}$ ($X^- = NCO^-$ or NCS^-) and anionic BPh_4^- species were found for both compounds. Bond distances and angles for both of the compounds are given in Tables VIII and IX.

As can be seen in Figures 2 and 3, the cations $[Mn_2(tren)_2(NCO)_2]^{2+}$ and $[Mn_2(tren)_2(NCS)_2]^{2+}$ are outer-sphere dimers similar to those we reported[3-5] for the analogous copper compounds. The outer-sphere association results from hydrogen bonding between two distorted trigonal-bipyramidal $[Mn(tren)(X)]^+$ moieties. In the case of the cyanate dimer, each cyanate ion binds with its nitrogen atom to one manganese ion. The oxygen atom of each cyanate ion is involved in hydrogen bonding with two tren nitrogen atoms bonded to the second manganese ion. These two hydrogen bonds are indicated in Figure 2 by dashed lines. The interatomic distances involved in the two hydrogen bonds are O–N(4)′ = 2.873 (7) and O–N(3)′ = 3.261 (6) Å. The corresponding hydrogen bonding distances are S–N(4)′ = 3.373 (5) and S–N(3)′ = 3.650 (5) Å for the thiocyanate compound, which has a similar hydrogen-bonding framework.

It is interesting to compare the structures of the two manganese outer-sphere dimers with those reported for the four $[Cu_2(tren)_2X_2]^{2+}$ analogues[3,19] and the one $[Zn_2(tren)_2Cl_2]^{2+}$ analogue;[20] see Table X. Two different outer-sphere dimers were noted for the copper compounds.[3,19] In

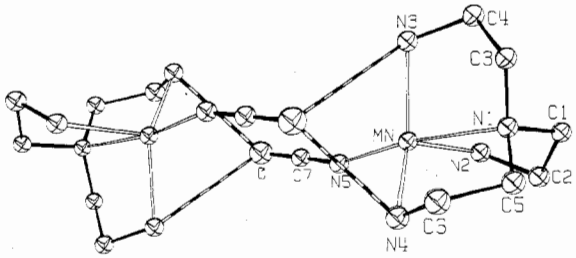

Figure 2. ORTEP plotting of $[Mn_2(tren)_2(NCO)_2]^{2+}$. Hydrogen atoms are not shown and possible hydrogen-bonding contacts for the oxygen atom of each NCO^- are indicated by dashed lines.

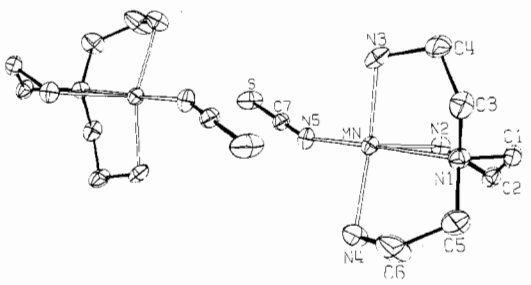

Figure 3. ORTEP plotting of $[Mn_2(tren)_2(NCS)_2]^{2+}$. Hydrogen atoms are not shown.

Table VI. Positional Parameters for All Atoms in $[Mn_2(tren)_2(NCS)_2](BPh_4)_2$ Including Isotropic Thermal Parameters for All Hydrogens[a]

Atom	x	y	z	Atom	x	y	z	B, Å²
Mn	0.14745 (4)	0.09613 (6)	0.09668 (3)	H(1)	0.2699	−0.0681	0.1642	5.0
N(1)	0.2631 (2)	0.2515 (3)	0.1317 (2)	H(2)	0.1860	−0.0639	0.2002	5.0
N(2)	0.2246 (2)	−0.0088 (4)	0.1790 (2)	H(3)	0.2062	0.1246	−0.0165	6.0
N(3)	0.2356 (3)	0.0811 (4)	0.0219 (2)	H(4)	0.2443	−0.0124	0.0120	6.0
N(4)	0.0726 (3)	0.2708 (4)	0.1285 (2)	H(5)	0.0594	0.2541	0.1715	6.6
N(5)	0.0465 (2)	−0.0519 (4)	0.0739 (2)	H(6)	0.0163	0.2816	0.1015	6.6
C(1)	0.3225 (3)	0.1877 (5)	0.1853 (2)	H(7)	0.3534	0.2559	0.2128	5.2
C(2)	0.2721 (3)	0.0908 (5)	0.2218 (2)	H(8)	0.3703	0.1363	0.1680	5.2
C(3)	0.3108 (3)	0.2775 (5)	0.0770 (2)	H(9)	0.2276	0.1429	0.2422	5.5
C(4)	0.3225 (4)	0.1501 (6)	0.0400 (2)	H(10)	0.3117	0.0489	0.2563	5.5
C(5)	0.2197 (4)	0.3741 (5)	0.1537 (3)	H(11)	0.3685	0.3179	0.0921	6.3
C(6)	0.1296 (5)	0.3920 (6)	0.1313 (4)	H(12)	0.2767	0.3398	0.0484	6.3
C(7)	0.0113 (3)	−0.1501 (5)	0.0563 (2)	H(13)	0.3641	0.0869	0.0681	7.0
S	−0.0379 (1)	−0.2915 (2)	0.03259 (9)	H(14)	0.3540	0.1667	0.0041	7.0
B	0.7237 (3)	0.2245 (4)	0.1304 (2)	H(15)	0.2544	0.4519	0.1421	7.4
C(11)	0.7219 (2)	0.0592 (3)	0.1389 (2)	H(16)	0.2256	0.3717	0.1992	7.4
C(12)	0.6421 (2)	−0.0152 (4)	0.1409 (2)	H(17)	0.1249	0.4234	0.0850	9.5
C(13)	0.6409 (3)	−0.1564 (4)	0.1410 (2)	H(18)	0.1031	0.4625	0.1524	9.5
C(14)	0.7188 (3)	−0.2291 (4)	0.1396 (2)	H(12b)[b]	0.5832	−0.2052	0.1428	4.8
C(15)	0.7990 (3)	−0.1604 (4)	0.1387 (2)	H(13b)	0.5854	0.0344	0.1411	3.9
C(16)	0.8000 (2)	−0.0192 (4)	0.1381 (2)	H(14b)	0.7187	−0.3266	0.1399	4.4
C(21)	0.7141 (2)	0.2467 (3)	0.0526 (2)	H(15b)	0.8547	−0.2099	0.1388	4.1
C(22)	0.6313 (3)	0.2203 (5)	0.0146 (2)	H(16b)	0.8574	0.0266	0.1371	3.4
C(23)	0.6191 (3)	0.2331 (5)	−0.0512 (2)	H(22b)	0.5801	0.1902	0.0351	4.5
C(24)	0.6905 (4)	0.2696 (5)	−0.0827 (2)	H(23b)	0.5604	0.2118	−0.0754	6.0
C(25)	0.7737 (3)	0.2911 (5)	−0.0480 (2)	H(24b)	0.6791	0.2822	−0.1292	5.9
C(26)	0.7852 (3)	0.2791 (4)	0.0184 (2)	H(25b)	0.8240	0.3174	−0.0703	5.1
C(31)	0.6400 (2)	0.3004 (4)	0.1603 (2)	H(26b)	0.8462	0.2938	0.0429	4.0
C(32)	0.6190 (2)	0.2653 (4)	0.2204 (2)	H(32b)	0.6524	0.1913	0.2425	3.7
C(33)	0.5543 (3)	0.3322 (4)	0.2496 (2)	H(33b)	0.5402	0.3033	0.2912	4.7
C(34)	0.5078 (3)	0.4399 (5)	0.2196 (3)	H(34b)	0.4615	0.4870	0.2386	5.0
C(35)	0.5258 (3)	0.4792 (4)	0.1599 (2)	H(35b)	0.4945	0.5564	0.1392	4.7
C(36)	0.5916 (2)	0.4093 (4)	0.1314 (2)	H(36b)	0.6034	0.4394	0.0898	3.9
C(41)	0.8154 (2)	0.2933 (4)	0.1700 (2)	H(42b)	0.8434	0.1481	0.2390	3.5
C(42)	0.8621 (3)	0.2364 (4)	0.2259 (2)	H(43b)	0.9637	0.2582	0.3009	5.0
C(43)	0.9332 (3)	0.3015 (5)	0.2635 (2)	H(44b)	1.0117	0.4746	0.2700	5.0
C(44)	0.9615 (3)	0.4272 (5)	0.2456 (2)	H(45b)	0.9375	0.5762	0.1796	4.7
C(45)	0.9176 (3)	0.4873 (4)	0.1914 (2)	H(46b)	0.8152	0.4667	0.1171	4.2
C(46)	0.8459 (3)	0.4216 (4)	0.1550 (2)					

[a] Estimated standard deviations of the least significant figure are shown in parentheses. [b] A small b designates hydrogens on the tetraphenylborate anion.

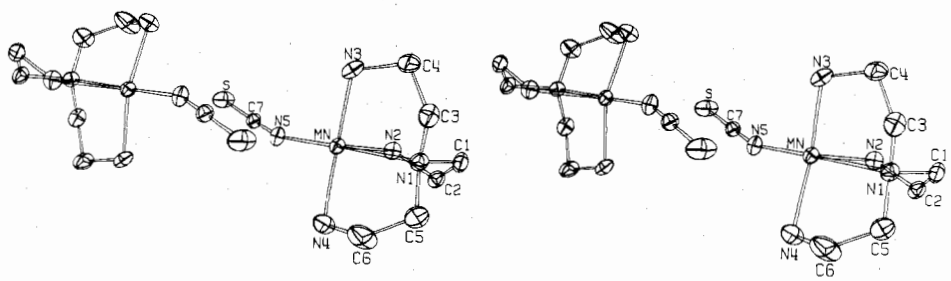

Figure 4. Stereoscopic view of $[Mn_2(tren)_2(NCS)_2]^{2+}$.

one type of copper dimer [$X^- = CN^-$, Cl^-, NCO^- (one of two different crystalline forms)] the X group is involved in only one hydrogen-bonding contact. In the second type of copper dimer ($X^- = NCS^-$) the two trigonal bipyramids are rotated relative to each other and the X group is involved in two hydrogen-bonding contacts. The second structural type is more compact with a shorter metal–metal distance than the first. The $[Zn_2(tren)_2Cl_2]^{2+}$ outer-sphere dimer has the first structure type, whereas both of the manganese outer-sphere dimers have the second type. A stereoscopic view of $[Mn_2(tren)_2(NCS)_2]^{2+}$ is illustrated in Figure 4. As would be expected, the Mn–N bond distances are all somewhat larger than the corresponding Cu–N bond distances as a result of the larger size of the Mn(II) ion. The most striking aspect of these structures is found in the displacement of the metal ions from the trigonal planes and the variation in axial bond lengths. Whereas the copper ions in all four copper structures are found to be about 0.23 Å above their trigonal planes, the zinc ion in $[Zn_2(tren)_2Cl_2]^{2+}$ is displaced by 0.38 Å and the two manganese ions by nearly 0.5 Å. The metal ion size seems to be the most important determining factor. As can be seen in Table X, an increase in the displacement of the metal ion from the trigonal plane is paralleled by a similar increase in the M–N(1) bond distance. It appears that the tren ligand is relatively rigid with respect to the distance of N(1) from the plane of the three primary amine nitrogen atoms. As a result, the 0.25-Å increase in metal–ion displacement in going from $[Cu_2(tren)_2(NCS)_2]^{2+}$ to $[Mn_2(tren)_2(NCS)_2]^{2+}$ is accompanied by a 0.30-Å increase in the M–N(1) distance.

The hydrogen bonding in these $[M_2(tren)_2X_2]^{2+}$ outer-sphere dimers has structural import. In all of the complexes there is a similar distortion of the trigonal-plane N–M–N angles. There is one small angle of about 112° and two larger angles of about 120°. On the other hand, the cation in [Mn-

Table VII. Anisotropic Thermal Parameters for $[Mn_2(tren)_2(NCS)_2](BPh_4)_2 \times 10^4$ [a]

Atom	B_{11}	B_{22}	B_{33}	B_{12}	B_{13}	B_{23}
Mn	49.9 (3)	113.8 (8)	26.0 (2)	−7.2 (4)	0.5 (2)	−10.5 (3)
N(1)	59 (2)	101 (4)	29 (1)	−9 (2)	7 (1)	−5 (2)
N(2)	63 (2)	124 (5)	30 (1)	−7 (3)	5 (1)	8 (2)
N(3)	101 (3)	167 (6)	21.0 (9)	−2 (3)	6 (1)	−11 (2)
N(4)	67 (2)	151 (6)	52 (2)	4 (3)	17 (2)	−6 (2)
M(5)	63 (2)	146 (5)	30 (1)	−17 (3)	−5 (1)	−1 (2)
C(1)	53 (2)	184 (7)	24 (1)	−26 (3)	−2 (1)	−7 (2)
C(2)	67 (3)	125 (6)	24 (1)	7 (3)	−3 (1)	−1 (2)
C(3)	74 (3)	176 (8)	31 (1)	−37 (4)	7 (2)	10 (3)
C(4)	81 (3)	240 (10)	28 (2)	−28 (5)	21 (2)	−7 (3)
C(5)	94 (4)	105 (7)	62 (2)	−8 (4)	8 (2)	−29 (3)
C(6)	97 (5)	110 (7)	109 (4)	15 (5)	28 (4)	−25 (4)
C(7)	48 (2)	149 (6)	26 (1)	−19 (3)	7 (1)	−8 (2)
S	93 (1)	205 (2)	65.0 (6)	−71 (1)	36.7 (7)	−54 (1)
B	34 (2)	78 (5)	18 (1)	2 (3)	2 (1)	3 (2)
C(11)	36 (2)	72 (4)	13.4 (8)	0 (2)	1 (1)	−1 (1)
C(12)	39 (2)	87 (5)	25 (1)	−1 (3)	6 (1)	−1 (2)
C(13)	61 (3)	95 (5)	26 (1)	−26 (3)	7 (1)	−2 (2)
C(14)	76 (3)	67 (5)	25 (1)	7 (3)	8 (1)	−2 (2)
C(15)	59 (3)	86 (5)	21 (1)	25 (3)	4 (1)	0 (2)
C(16)	39 (2)	93 (5)	16.4 (9)	4 (3)	2 (1)	−1 (2)
C(21)	38 (2)	73 (4)	20 (1)	7 (2)	1 (1)	0 (2)
C(22)	49 (2)	142 (6)	22 (1)	0 (3)	−2 (1)	1 (2)
C(24)	106 (4)	140 (7)	18 (1)	34 (4)	3 (2)	7 (2)
C(25)	79 (3)	115 (6)	24 (1)	21 (3)	16 (2)	14 (2)
C(26)	51 (2)	96 (5)	21 (1)	4 (3)	7 (1)	4 (2)
C(31)	26 (2)	65 (4)	21 (1)	−6 (2)	0 (1)	−5 (2)
C(32)	38 (2)	88 (5)	24 (1)	0 (3)	5 (1)	−3 (2)
C(33)	46 (2)	115 (6)	30 (1)	−8 (3)	15 (1)	−11 (2)
C(34)	39 (2)	116 (6)	44 (2)	−3 (3)	17 (2)	−19 (3)
C(35)	38 (2)	78 (5)	44 (2)	10 (3)	1 (2)	−5 (2)
C(36)	38 (2)	81 (4)	26 (1)	−2 (3)	2 (1)	1 (2)
C(41)	27 (2)	66 (4)	20 (1)	7 (2)	4 (1)	−3 (2)
C(42)	41 (2)	79 (4)	22 (1)	1 (2)	−1 (1)	−4 (2)
C(43)	48 (2)	128 (6)	26 (1)	28 (3)	−10 (1)	−15 (2)
C(44)	38 (2)	124 (6)	40 (2)	−3 (3)	−5 (1)	−28 (3)
C(45)	44 (2)	86 (5)	39 (2)	−16 (3)	6 (2)	−11 (2)
C(46)	40 (2)	71 (5)	28 (1)	3 (2)	3 (1)	−1 (2)

[a] The form of the anisotropic thermal ellipsoid is given by $B_{11}h^2 + B_{22}k^2 + B_{33}l^2 + B_{12}hk + B_{13}hl + B_{23}kl$. Estimated standard deviations of the least significant figure are given in parentheses.

$(Me_6tren)Br]Br$ contains a threefold axis of symmetry with all three N(ax)–Mn–N(ax) angles being 117.4°. Furthermore, it is important to note that the manganese ion in monomeric $Mn(Me_6tren)Br^+$ is displaced by only 0.36 Å from the trigonal plane.[11]

The geometries of the BPh_4^- ion in all of the $[M_2(tren)_2X_2](BPh_4)_2$ compounds are very similar. Least-squares planes for the phenyl groups of the BPh_4^- ions in the two manganese compounds are given in Tables XI and XII.[13] The phenyl rings are all essentially planar with a slight distortion from a regular hexagon as found previously.[3,19]

Three other cases of trigonal-bypyramidal Mn(II) complexes have been structurally characterized. If an aqueous solution of $Mn(ClO_4)_2 \cdot 6H_2O$ is allowed to sit in contact with single crystals of zeolite A, a compound of unit cell stoichiometry $[Mn_{4.5}Na_3(Si_{12}Al_{12}O_{48})] \cdot xH_2O$ is obtained. Single-crystal x-ray diffraction studies of this compound in both the hydrated and dehydrated forms have been performed.[6] The Mn^{2+} ions occupy, in either case, threefold axis sites near the six-oxygen "windows" of the zeolite. In the hydrated form, two water molecules are bonded in the axial positions to complete the trigonal-bipyramidal coordination sphere. The manganese ion lies 0.24 (3) Å from the trigonal plane in the hydrated form. In the anhydrous form, this distance is only 0.11 (3) Å so the trigonal site appears to be slightly too small to accommodate the Mn^{2+} ion in a planar environment.

The compound $Mn(PPA)Cl_2$, where PPA is 2-[*N*-(3-(2-pyridyl)-2-picolyl)imino]-4-oxo-1,2,3,4-tetrahydroquinazoline, has also been shown to be trigonal bipyramidal, although somewhat distorted.[7] The trigonal plane is defined by the two chlorine atoms and the imine nitrogen of the ligand. The complex is appreciably distorted from a trigonal bipyramid; e.g., the axial–metal–axial angle is only 139.9 (1)°. No value was given for the deviation of the manganese ion from the trigonal plane.

The only other trigonal-bipyramidal Mn(II) compound which has been structurally characterized is dichlorotris(2-methylimidazole)manganese(II).[8] In this complex, the trigonal plane is composed of two nitrogen atoms from two methylimidazole groups and a chlorine atom. The trigonal plane shows considerable distortion with the three basal angles being 110, 119, and 131°. The axial ligand–metal–axial ligand angle is 168°. The manganese ion sits in the trigonal plane.

Bis(2,2′-biquinolyl)di-μ-chloro-dimanganese(II) is the only dimeric five-coordinate manganese(II) compound for which a structure has been reported.[12] The coordination geometry at each Mn(II) ion in this dimer exhibits extreme distortion from both trigonal-bipyramidal and square-pyramidal geometries. The metal–metal distance is 3.776 (1) Å.

Infrared Measurements. Infrared spectra were obtained for the $[Mn_2(tren)_2X_2](BPh_4)_2$ ($X^- = NCO^-$, NCS^-, CN^-, Cl^-, Br^-, and N_3^-) compounds, run as KBr pellets at room temperature. It has been our experience that the pattern of N–H stretches centered about 3300 cm^{-1} and the pattern of H–N–H bending vibrations of the tren ligand in the region of 1200–1300 cm^{-1} are characteristic of the coordination geometry (i.e., whether it is five- or six-coordinate) at the metal ion. A careful analysis[21] of these infrared patterns for the above six manganese compounds shows that, in addition to the structurally characterized NCO^- and NCS^- compounds, the

Table VIII. Molecular Distances (Å) and Angles (deg) for $[Mn_2(tren)_2(NCO)_2](BPh_4)_2$[a]

Distances within $[Mn_2(tren)_2(NCO)_2]^{2+}$

Mn-Mn′	5.893 (1)	C(1)-C(2)	1.504 (8)
Mn-N(1)	2.412 (4)	C(3)-C(4)	1.496 (9)
Mn-N(2)	2.206 (5)	C(5)-C(6)	1.50 (1)
Mn-N(3)	2.186 (4)	C(2)-N(2)	1.468 (7)
Mn-N(4)	2.197 (5)	C(4)-N(3)	1.477 (7)
Mn-N(5)	2.051 (5)	C(6)-N(4)	1.467 (8)
N(1)-C(1)	1.483 (7)	C(7)-N(5)	1.157 (8)
N(1)-C(3)	1.466 (7)	C(7)-O	1.203 (8)
N(1)-C(5)	1.466 (7)	O-N(3)′	3.261 (6)
		O-N(4)′	2.873 (7)

Angles within $[Mn_2(tren)_2(NCO)_2]^{2+}$

N(1)-Mn-N(2)	75.6 (2)	N(1)-C(1)-C(2)	111.1 (5)
N(1)-Mn-N(3)	76.5 (2)	N(1)-C(3)-C(4)	111.4 (5)
N(1)-Mn-N(4)	76.1 (2)	N(1)-C(5)-C(6)	111.0 (5)
N(5)-Mn-N(1)	171.3 (2)	C(1)-C(2)-N(2)	109.7 (5)
N(5)-Mn-N(2)	100.0 (2)	C(5)-C(6)-N(4)	110.9 (5)
N(5)-Mn-N(3)	112.0 (2)	C(2)-N(2)-Mn	110.6 (3)
N(5)-Mn-N(4)	99.7 (2)	C(4)-N(3)-Mn	112.5 (3)
N(2)-Mn-N(3)	105.0 (2)	C(6)-N(4)-Mn	110.2 (4)
N(2)-Mn-N(4)	121.5 (2)	C(1)-N(1)-C(3)	111.9 (4)
Mn-N(1)-C(1)	107.9 (3)	C(1)-N(1)-C(5)	111.5 (4)
Mn-N(1)-C(3)	105.7 (3)	C(3)-N(1)-C(5)	112.1 (4)
Mn-N(1)-C(5)	107.5 (3)	N(5)-C(7)-O	178.8 (7)
Mn-N(5)-C(7)	158.3 (5)	O-N(3)′-Mn′	65.1 (1)

Distances in Tetraphenylborate Anion

C(11)-C(12)	1.390 (8)	C(31)-C(32)	1.411 (8)
C(12)-C(13)	1.381 (9)	C(32)-C(33)	1.385 (8)
C(13)-C(14)	1.37 (1)	C(33)-C(34)	1.37 (1)
C(14)-C(15)	1.38 (1)	C(34)-C(35)	1.38 (1)
C(15)-C(16)	1.380 (9)	C(35)-C(36)	1.384 (9)
C(16)-C(11)	1.409 (8)	C(36)-C(31)	1.381 (8)
C(21)-C(22)	1.394 (8)	C(41)-C(42)	1.397 (8)
C(22)-C(23)	1.389 (8)	C(42)-C(43)	1.389 (8)
C(23)-C(24)	1.391 (9)	C(43)-C(44)	1.37 (1)
C(24)-C(25)	1.367 (9)	C(44)-C(45)	1.39 (1)
C(25)-C(26)	1.375 (8)	C(45)-C(46)	1.391 (9)
C(26)-C(21)	1.400 (8)	C(46)-C(41)	1.395 (8)
B-C(11)	1.645 (8)	B-C(31)	1.637 (8)
B-C(21)	1.662 (8)	B-C(41)	1.634 (8)

Angles in the Tetraphenylborate Anion

C(16)-C(11)-C(12)	114.4 (5)	C(36)-C(31)-C(32)	114.4 (5)
C(11)-C(12)-C(13)	123.8 (5)	C(31)-C(32)-C(33)	123.1 (5)
C(12)-C(13)-C(14)	119.6 (6)	C(32)-C(33)-C(34)	119.7 (6)
C(13)-C(14)-C(15)	119.3 (6)	C(33)-C(34)-C(35)	119.4 (6)
C(14)-C(15)-C(16)	120.2 (6)	C(34)-C(35)-C(36)	119.7 (6)
C(15)-C(16)-C(17)	122.6 (5)	C(35)-C(36)-C(31)	123.7 (5)
C(26)-C(21)-C(22)	115.4 (5)	C(46)-C(41)-C(42)	114.0 (5)
C(21)-C(22)-C(23)	123.2 (5)	C(41)-C(42)-C(43)	123.5 (5)
C(22)-C(23)-C(24)	118.9 (5)	C(42)-C(43)-C(44)	120.0 (6)
C(23)-C(24)-C(25)	119.2 (5)	C(43)-C(44)-C(45)	119.6 (7)
C(24)-C(25)-C(26)	121.2 (5)	C(44)-C(45)-C(46)	118.4 (6)
C(25)-C(26)-C(21)	122.0 (5)	C(45)-C(46)-C(41)	124.5 (5)
B-C(11)-C(12	121.7 (5)	C(11)-B-C(21)	102.9 (4)
B-C(11)-C(16)	123.5 (5)	C(11)-B-C(31)	110.6 (4)
B-C(21)-C(22)	121.5 (5)	C(11)-B-C(41)	115.3 (4)
B-C(21)-C(26)	122.9 (5)	C(21)-B-C(31)	111.4 (4)
B-C(31)-C(32)	120.0 (5)	C(21)-B-C(41)	111.5 (4)
B-C(31)-C(36)	125.3 (5)	C(31)-B-C(41)	105.3 (4)
B-C(41)-C(42)	125.1 (5)		
B-C(41)-C(46)	120.5 (5)		

[a] Estimated standard deviations of the least significant figures are in parentheses.

Table IX. Molecular Distances (Å) and Angles (deg) for $[Mn_2(tren)_2(NCS)_2](BPh_4)_2$[a]

Distances within $[Mn_2(tren)_2(NCS)_2]^{2+}$

Mn-Mn′	5.8729 (8)	C(1)-C(2)	1.493 (6)
Mn-N(1)	2.343 (3)	C(3)-C(4)	1.499 (8)
Mn-N(2)	2.201 (4)	C(5)-C(6)	1.37 (1)
Mn-N(3)	2.194 (4)	C(2)-N(2)	1.449 (6)
Mn-N(4)	2.203 (4)	C(4)-N(3)	1.464 (7)
Mn-N(5)	2.100 (4)	C(6)-N(4)	1.461 (7)
N(1)-C(1)	1.475 (6)	C(7)-N(5)	1.136 (6)
N(1)-C(3)	1.460 (6)	C(7)-S	1.619 (5)
N(1)-C(5)	1.474 (6)	S-N(3)′	3.650 (5)
		S-N(4)′	3.373 (5)

Angles within $[Mn_2(tren)_2(NCS)_2]^{2+}$

N(1)-Mn-N(2)	77.2 (1)	N(1)-C(3)-C(4)	111.7 (4)
N(1)-Mn-N(3)	77.5 (1)	N(1)-C(5)-C(6)	116.6 (5)
N(1)-Mn-N(4)	77.0 (1)	C(1)-C(2)-N(2)	110.2 (4)
N(5)-Mn-N(1)	174.6 (1)	C(3)-C(4)-N(3)	111.2 (4)
N(5)-Mn-N(2)	97.6 (1)	C(5)-C(6)-N(4)	116.4 (6)
N(5)-Mn-N(3)	105.6 (1)	C(2)-N(2)-Mn	109.3 (3)
N(5)-Mn-N(4)	103.6 (2)	C(4)-N(3)-Mn	112.1 (3)
N(2)-Mn-N(3)	103.7 (1)	C(6)-N(4)-Mn	109.5 (4)
N(2)-Mn-N(4)	110.8 (1)	C(1)-N(1)-C(3)	112.0 (3)
N(3)-Mn-N(4)	130.6 (2)	C(1)-N(1)-C(5)	110.4 (4)
Mn-N(1)-C(1)	107.4 (2)	C(3)-N(1)-C(5)	112.8 (4)
Mn-N(1)-C(3)	106.4 (3)	N(5)-C(7)-S	178.8 (4)
Mn-N(1)-C(5)	107.4 (3)	S-N(3)′-Mn	69.6 (1)
Mn-N(5)-C(7)	161.2 (4)	S-N(4)′-Mn′	75.7 (1)
N(1)-C(1)-C(2)	112.2 (4)		

Distances in Tetraphenylborate Anion

C(11)-C(12)	1.401 (5)	C(31)-C(32)	1.394 (5)
C(12)-C(13)	1.390 (6)	C(32)-C(33)	1.381 (6)
C(13)-C(14)	1.366 (7)	C(33)-C(34)	1.372 (6)
C(14)-C(15)	1.374 (6)	C(34)-C(35)	1.379 (7)
C(15)-C(16)	1.391 (6)	C(35)-C(36)	1.399 (6)
C(16)-C(11)	1.396 (5)	C(36)-C(31)	1.385 (5)
C(21)-C(22)	1.398 (6)	C(41)-C(42)	1.400 (5)
C(22)-C(23)	1.381 (6)	C(42)-C(43)	1.388 (6)
C(23)-C(24)	1.378 (8)	C(43)-C(44)	1.377 (7)
C(24)-C(25)	1.364 (8)	C(44)-C(45)	1.371 (7)
C(25)-C(26)	1.392 (6)	C(45)-C(46)	1.384 (6)
C(26)-C(21)	1.398 (5)	C(46)-C(41)	1.394 (5)
B-C(11)	1.638 (5)	B-C(31)	1.652 (5)
B-C(21)	1.643 (5)	B-C(41)	1.644 (5)

Angles in the Tetraphenylborate Anion

C(16)-C(11)-C(12)	114.9 (3)	C(36)-C(31)-C(32)	115.0 (3)
C(11)-C(12)-C(13)	122.3 (4)	C(31)-C(32)-C(33)	123.3 (4)
C(12)-C(13)-C(14)	120.8 (4)	C(32)-C(33)-C(34)	120.0 (4)
C(13)-C(14)-C(15)	119.0 (4)	C(33)-C(34)-C(35)	119.3 (4)
C(14)-C(15)-C(16)	120.1 (4)	C(34)-C(35)-C(36)	119.5 (4)
C(15)-C(16)-C(11)	122.9 (3)	C(35)-C(36)-C(31)	122.9 (4)
C(26)-C(21)-C(22)	114.6 (3)	C(46)-C(41)-C(42)	114.6 (3)
C(21)-C(22)-C(23)	122.8 (4)	C(41)-C(42)-C(43)	123.1 (4)
C(22)-C(23)-C(24)	120.5 (5)	C(42)-C(43)-C(44)	119.8 (4)
C(23)-C(24)-C(25)	118.9 (5)	C(43)-C(44)-C(45)	119.2 (4)
C(24)-C(25)-C(26)	120.2 (4)	C(44)-C(45)-C(46)	120.2 (4)
C(25)-C(26)-C(21)	122.9 (4)	C(45)-C(46)-C(41)	123.1 (4)
B-C(11)-C(12)	123.3 (3)	C(11)-B-C(21)	104.0 (3)
B-C(11)-C(16)	121.4 (3)	C(11)-B-C(31)	122.5 (3)
B-C(21)-C(22)	119.7 (3)	C(11)-B-C(41)	122.2 (3)
B-C(21)-C(26)	125.4 (3)	C(21)-B-C(31)	110.9 (3)
B-C(31)-C(32)	120.9 (3)	C(21)-B-C(41)	113.8 (3)
B-C(31)-C(36)	123.8 (3)	C(31)-B-C(41)	103.6 (3)
B-C(41)-C(42)	122.9 (3)		
B-C(41)-C(46)	122.1 (3)		

[a] Estimated standard deviations of the least significant figures are in parentheses.

CN^-, Cl^-, and Br^- compounds also have five-coordinate manganese ions. The two infrared regions are different in appearance for the N_3^- compound and it is concluded that the manganese ions in this compound are most likely six-coordinate as a result of inner-sphere bridging by the two N_3^- ions.

Magnetic Susceptibility and EPR of Monomeric [Mn(Me$_6$tren)X]X Species. In order to assist in understanding the complicated EPR spectra and the magnetic susceptibility data for the outer-sphere Mn–tren compounds, the characteristics of similar known monomeric trigonal-bipyramidal Mn(II) complexes were sought. The structure of [Mn(Me$_6$tren)Br]Br has been reported.[11] In this monomeric compound, the manganese ion sits on a site of (crystallographically imposed)

Table X. Distances (Å) and Angles (deg) in Compounds of Composition $[M_2(tren)_2X_2](BPh_4)_2$

	$M^{2+} = Mn^{2+}$ $X^- = NCS^-$	$M^{2+} = Cu^{2+}$ $X^- = NCS^-$	$M^{2+} = Mn^{2+}$ $X^- = NCO^-$	$M^{2+} = Cu^{2+}$ $X^- = NCO^-$	$M^{2+} = Zn^{2+}$ [a] $X^- = Cl^-$	$M^{2+} = Cu^{2+}$ $X^- = Cl^-$
Structure type	1	1	1	2	2	2
M-N(ax)	2.343 (3)	2.047 (6)	2.412 (4)	2.06 (1)	2.325 (7)	2.081 (3)
M-N(eq)	2.201 (4)	2.088 (6)	2.206 (5)	2.10 (1)	2.068 (7)	2.099 (3)
	2.194 (4)	2.075 (6)	2.186 (4)	2.08 (1)	2.063 (7)	2.107 (3)
	2.203 (4)	2.060 (5)	2.197 (5)	2.08 (1)	2.065 (6)	2.066 (3)
M-X(bridge)	2.100 (4)	1.946 (7)	2.051 (5)	1.87 (1)	2.308 (5)	2.253 (1)
N(ax)-M-X	174.6 (1)	179.0 (2)	171.3 (2)	176.7 (6)	176.4 (2)	177.8 (1)
N(ax)-M-N(eq)	77.2 (1)	83.6 (2)	75.6 (2)	83.5 (5)	79.6 (2)	83.0 (1)
	77.5 (1)	84.0 (2)	76.5 (2)	84.8 (5)	79.0 (3)	83.4 (1)
	77.0 (1)	84.0 (2)	76.1 (2)	83.1 (5)	78.7 (3)	83.8 (1)
Distance of M from trigonal plane	0.4721	0.2216 (8)	0.5275	0.231 (2)	0.38	0.2402 (4)
M-M	5.8729 (8)	6.136 (1)	5.893 (1)	6.540 (2)	5.6861 (8)	5.7994 (6)
X-N	3.650 (5)	3.736 (7)	3.261 (6)	2.95 (1)	3.334 (4)	3.368 (4)
	3.373 (5)	3.463 (6)	2.873 (7)			
X-H	2.9872	2.923 (2)			2.58 (4)	2.467 (1)
	2.9096	2.790 (2)				

[a] Reference 20.

threefold symmetry and is trigonal bipyramidal. X-Band EPR spectra were obtained for powdered samples of [Mn(Me$_6$tren)Br]Br and [Mn(Me$_6$tren)I]I and are illustrated in Figure 5. Both spectra show similar broad resonances with the greatest intensity resonances occurring at very low fields. Similar complex, broad spectra have been observed[22-24] for distorted Mn(II) compounds.

Doping a small amount of Mn(II) into [Zn(Me$_6$tren)I]I gave a nicely resolved X-band EPR spectrum for a powdered sample, as indicated by tracing C in Figure 5. Four resonances are seen, each structured by manganese hyperfine patterns. It is interesting to note that there is an alternating line width behavior. The hyperfine pattern centered at ~1070 G consists of narrow lines, the hyperfine pattern at 3200 G is quite broad while the pattern at ~5020 G is fairly well resolved, and finally the pattern at ~7650 G is again broad. Such a line width alternation has been noted before and is due to a variation in spin–lattice relaxation times for the different transitions. Dowsing and Gibson[25] have plotted the expected EPR transitions for a high-spin d^5 ion experiencing various magnitudes of zero-field splitting. The manganese ion site is presumably axial when doped into [Zn(Me$_6$tren)I]I so the rhombic zero-field splitting parameter $E = 0$ and only the axial zero-field splitting parameter D is nonzero (spin Hamiltonian is $D\hat{S}_z^2$). Using the various plots, it is estimated that the value of D is 0.20 cm^{-1}. Table XIII gives the assignment for the X-band EPR features and the corresponding calculated resonance fields as gleaned from these plots. It can be seen that there is reasonably good agreement.

The Q-band EPR spectrum of Mn^{2+} doped into [Zn(Me$_6$tren)I]I is illustrated in Figure 6. Again, the features of the spectrum can be accounted for in an approximate manner by taking $D = 0.20$ cm^{-1}; see Table XIII. It should be noted, however, that there are a larger number of hyperfine lines than can be accounted for in this simple analysis. It is possible that, in doping Mn^{2+} into the zinc host, more than one type of site exist and this gives rise to "extra" transitions at slightly different fields. At X-band frequencies, the separation between these transition fields is insufficient to be resolved. Figure 7 shows the Q-band EPR spectra of powdered, undoped samples of [Mn(Me$_6$tren)I]I and [Mn(Me$_6$tren)Br]Br. As with the X-band spectra, broad overlapping resonances are seen which make it difficult to analyze the spectra.

The magnetic susceptibility data for [Mn(Me$_6$tren)Br]Br are given in Table XIV[13] and plotted in Figure 8. The effective magnetic moment, μ_{eff}, is relatively constant at 6.0 ± 0.1 μ_B except for a drop at low temperatures. The theoretical

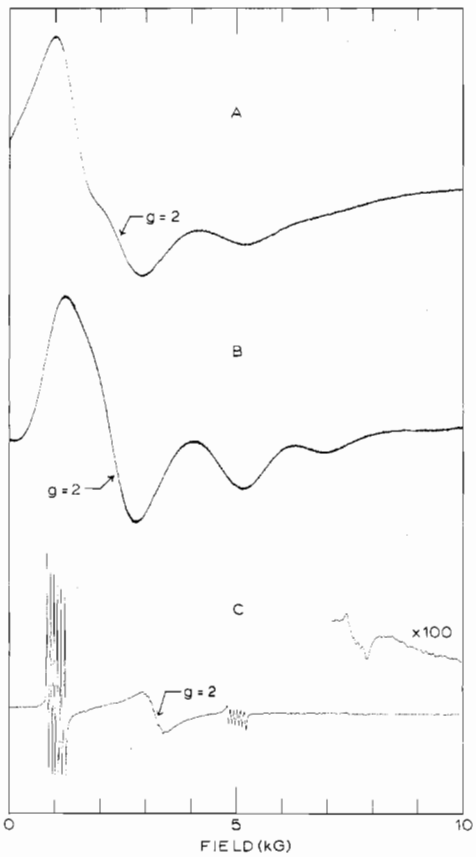

Figure 5. Room-temperature X-band EPR spectra of powdered samples of (A) [Mn(Me$_6$tren)Br]Br, (B) [Mn(Me$_6$tren)I]I, and (C) Mn^{2+} doped into [Zn(Me$_6$tren)I]I.

approach used for least-squares fitting of the data for a high-spin d^5 monomer with axial symmetry is described in the Appendix. Direct matrix diagonalization, rather than a perturbation approach, was used. Three parameters, $g_\parallel$, $g_\perp$, and the zero-field splitting parameter D were used and it is gratifying to see that reasonable values are obtained from this fit ($g_\parallel = 1.97$, $g_\perp = 2.07$, and $D = 0.24$ cm^{-1}). The value of D obtained from this fitting is quite similar to that obtained from the EPR spectrum of the doped sample of [Mn(Me$_6$tren)I]I. At the very least, Figure 8 illustrates the theoretical μ_{eff} vs. temperature curve expected for a monomeric system with $D \approx 0.2$ cm^{-1}.

Magnetic Susceptibility and EPR Spectra of [Mn$_2$-

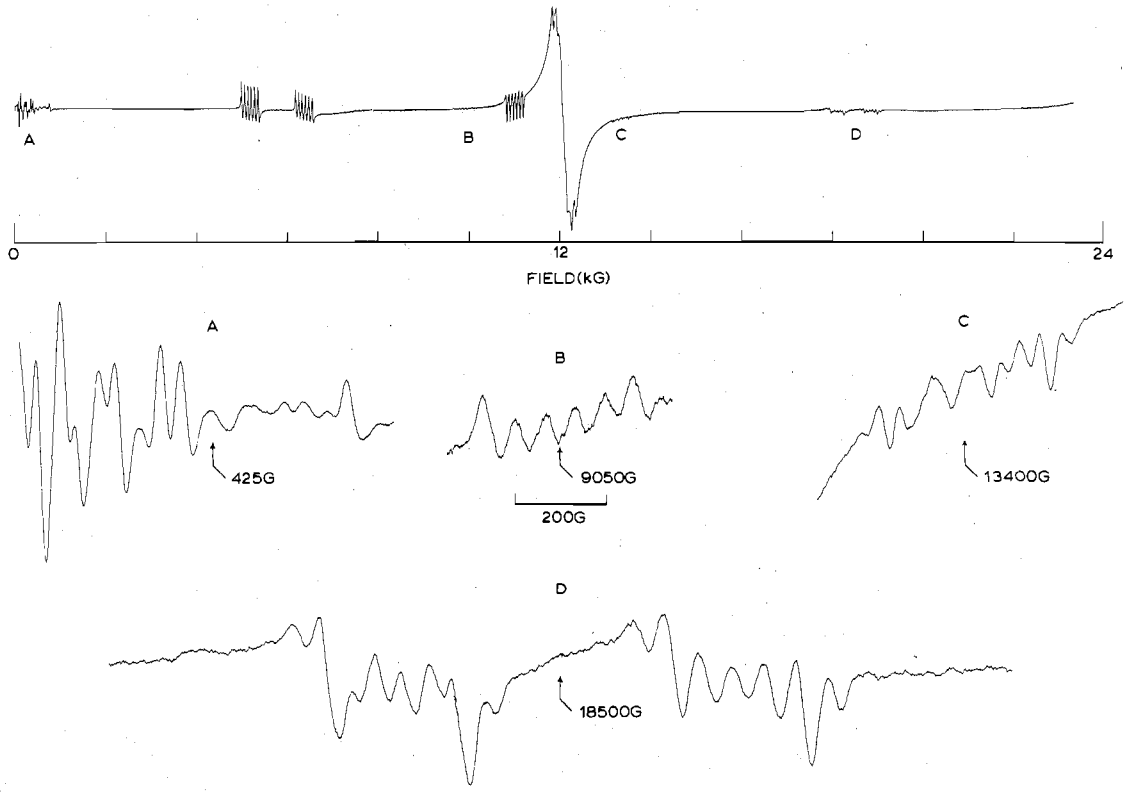

Figure 6. Room-temperature Q-band EPR spectrum of a powdered sample of Mn^{2+}-doped $[Zn(Me_6tren)I]I$.

Table XIII. EPR Transitions for $[Mn(Me_6tren)I]I$ Doped into $[Zn(Me_6tren)I]I$ ($D = 0.20$ cm^{-1}, $E = 0.0$ cm^{-1})

Transition (axis)	Calcd field,[a] G	Obsd field, G
	X Band	
$-3/2 \rightarrow -5/2$ (x, y)	1 000	1 070
$-1/2 \rightarrow -3/2$ (z)	1 100	1 078
$1/2 \rightarrow -1/2$ (x, y)	3 200	3 200
$1/2 \rightarrow -1/2$ (z)	3 200	3 200
Unspecified (z)[b]	5 000	5 020
$3/2 \rightarrow 1/2$ (z)	7 600	7 650
$5/2 \rightarrow 3/2$ (x, y)	7 700	7 650
$5/2 \rightarrow 3/2$ (z)	11 800	[c]
	Q Band	
$-3/2 \rightarrow -5/2$ (z)	0	<800
Unspecified (x, y)[b]	0	<800
Unspecified (z)[b]	6 100	5 175
$-1/2 \rightarrow -3/2$ (z) and $-3/2 \rightarrow -5/2$ (x, y)	6 300	6 375
$-1/2 \rightarrow -3/2$ (x, y)	9 300	9 095
$1/2 \rightarrow -1/2$ (x, y)	11 400	11 000
$1/2 \rightarrow -1/2$ (z)	11 680	12 000
$3/2 \rightarrow 1/2$ (x, y)	13 800	13 400
$3/2 \rightarrow 1/2$ (z)	17 900	18 100
$5/2 \rightarrow 3/2$ (x, y)	18 900	18 900
$5/2 \rightarrow 3/2$ (z)	24 500	[c]

[a] From figures in ref 25. [b] Allowed due to mixing of states. [c] Beyond scan capabilities of instrument.

$(tren)_2X_2]^{2+}$ Outer-Sphere Complexes. Two $S = 5/2$ ions couple in an exchange interaction to give dimer states with a total spin of $S = 5, 4, 3, 2, 1$, or 0. Each state, except the $S = 0$ state, has a degeneracy $(2S + 1)$ greater than one and, as has been pointed out by several workers,[26,27] may have a different zero-field splitting. Thus, there are a total of 30 possible allowed transitions ($\Delta M_s = 1$) for each magnetic field orientation, which gives in total 90 $\Delta M_s = 1$ transitions. There is also the possibility of observing many transitions with $\Delta M_s \neq 1$.[28,29] For a magnetically concentrated sample, where the line width of the absorptions is large, severe overlap problems may arise, making detailed quantitative interpretation next to impossible. The BPh_4^- counterions do provide some degree of magnetic dilution.

Figure 9 shows the X-band EPR spectra of a powdered sample of $[Mn_2(tren)_2(NCO)_2](BPh_4)_2$ as a function of temperature. When compared to the room-temperature X-band spectra of the monomeric complexes as pictured in Figure 5, the 300 K spectrum of this outer-sphere cyanate dimer looks different. The dimer spectrum exhibits more features which are more closely spaced. Also, in the dimer spectrum the relatively intense absorptions at fields less than ~3200 G exhibit a marked temperature dependence. Although the BPh_4^- counterion provides some degree of magnetic dilution, it is insufficient to provide well-resolved spectra of the cyanate dimer. The room-temperature Q-band spectrum of a powdered sample of $[Mn_2(tren)_2(NCO)_2](BPh_4)_2$, given in Figure 10, also appears to differ from the monomer Q-band spectra in Figure 7 in that there are a greater number of closely spaced features. The most intense feature in both the X-band and Q-band spectra of $[Mn_2(tren)_2(NCO)_2](BPh_4)_2$ occurs at $g = 2.0$. At present, it is *not* possible to give an assignment for the many features that are seen in the EPR spectra of the cyanate dimer. Because the spectra do appear different from the relatively simple monomer spectra, it would seem that at this point it could be concluded that there is an exchange interaction present in the cyanate outer-sphere dimer. Before the EPR results for the other outer-sphere dimers are presented, the magnetic susceptibility results will be summarized.

Figure 11 and Table XV[13] present the variable-temperature magnetic susceptibility results for $[Mn_2(tren)_2(NCO)_2](BPh_4)_2$. The μ_{eff} per manganese ion varies from 5.91 μ_B at 296 K to 4.85 μ_B at 4.2 K. As can be seen, the μ_{eff}/Mn value is attenuated considerably more at low temperatures than was observed for $[Mn(Me_6tren)Br]Br$; see Figure 8. The theoretical expressions used to fit the magnetic susceptibility data for an exchange-interacting $S_1 = S_2 = 5/2$ dimer including

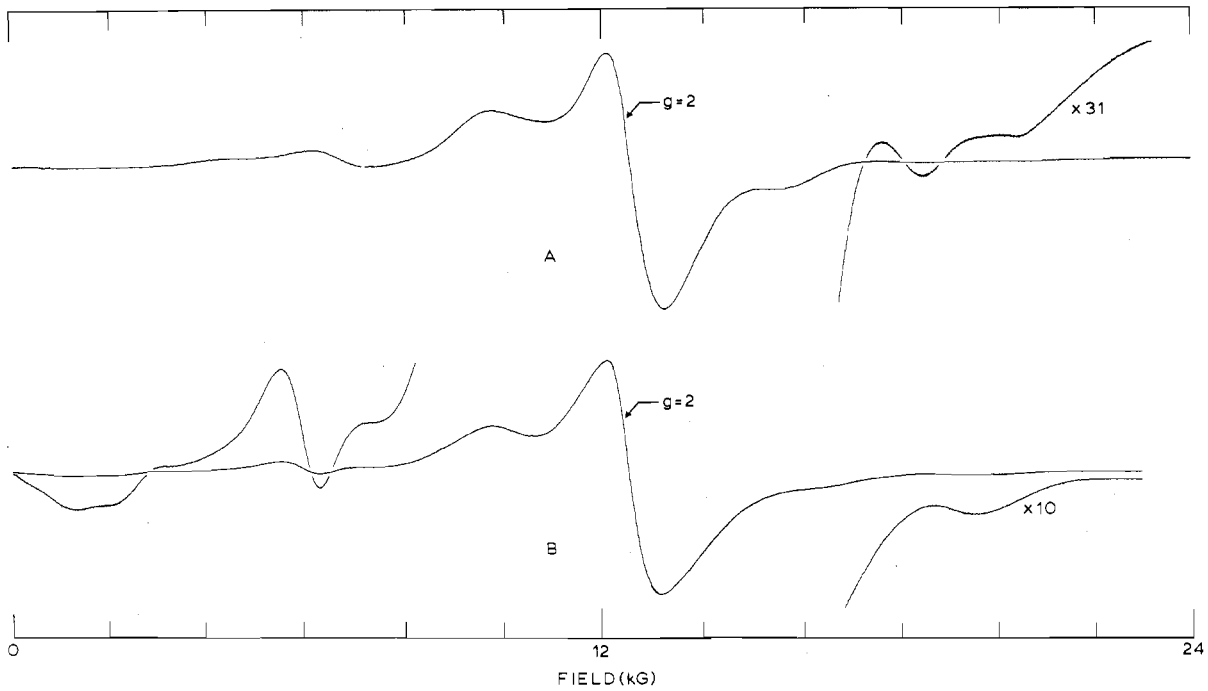

Figure 7. Room-temperature Q-band EPR spectra of powdered samples of (A) [Mn(Me$_6$tren)I]I and (B) [Mn$_2$(Me$_6$tren)Br]Br.

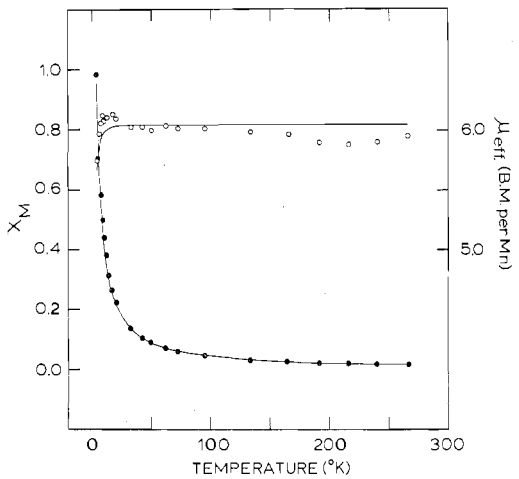

Figure 8. Molar paramagnetic susceptibility (cgsu/mol) and effective magnetic moment (μ_{eff} in μ_B) vs. temperature curves for [Mn(Me$_6$tren)Br]Br.

single-ion zero-field splitting are detailed in the Appendix. An isotropic exchange interaction was assumed as was the presence of axial zero-field splitting [i.e., only $D\hat{S}_z^2$].

The susceptibility data for $[Mn_2(tren)_2(NCO)_2](BPh_4)_2$ were least-squares fit (via matrix-diagonalization techniques) to the equations for both a monomer and a dimer. In Figure 11, the solid lines represent the fit to the dimer equations. Although the fit to the monomer equations is actually better [as indicated by a smaller value of $S = (\chi_{obsd} - \chi_{calcd})^{1/2}/(n - m)$, where n is the number of data points and m is the number of parameters], the values for the monomer parameters are unreasonable, with $D = 3.8$ cm^{-1}, $g_{\|} = 2.20$, and $g_{\perp} = 1.91$. The zero-field splitting parameter is unreasonable, because a monomeric $S = {}^5/_2$ compound with such a large D value should give an EPR spectrum with $g_{\|} = 2$ and $g_{\perp} = 6$, which is clearly *not* what is observed. The zero-field splitting in these compounds is due largely to spin–orbit admixture of excited states into the $^6A_1$ single-ion ground state with a very minor contribution from low-symmetry crystal fields. In fact, the zero-field splitting is a single-ion property even for the outer-sphere dimers, because with the very appreciable metal–metal distances the interion dipolar zero-field splitting is negligible. Furthermore, the $D = 3.8$ cm^{-1} value from the fitting to the monomer equations is unreasonable in light of the $D = 0.20$ cm^{-1} value found from the EPR spectrum of

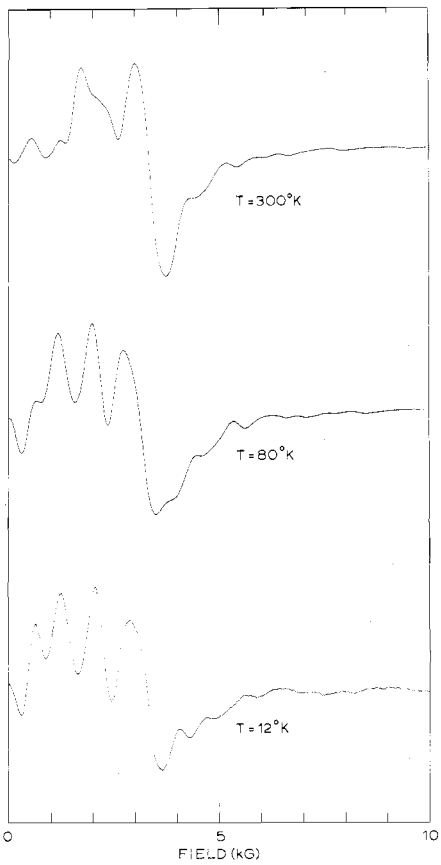

Figure 9. X-Band EPR spectra of a powdered sample of $[Mn_2(tren)_2(NCO)_2](BPh_4)_2$ at three different temperatures.

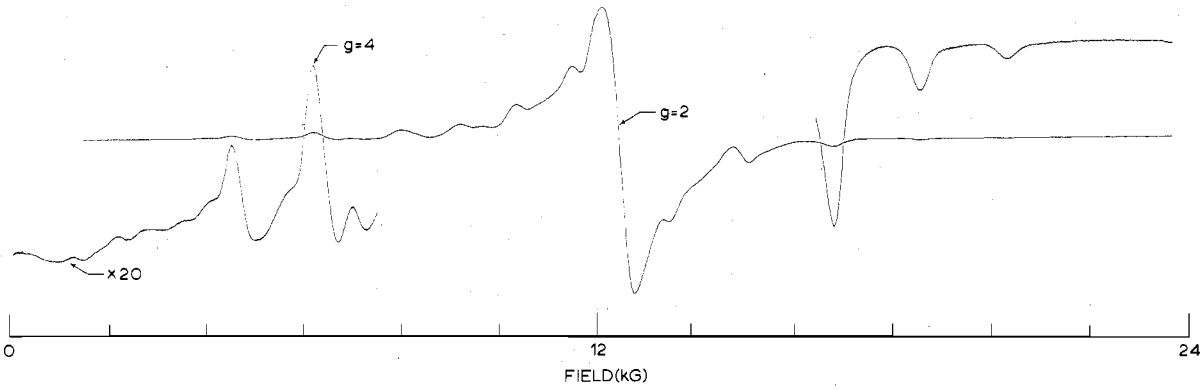

Figure 10. Room-temperature Q-band EPR spectrum of $[Mn_2(tren)_2(NCO)_2](BPh_4)_2$.

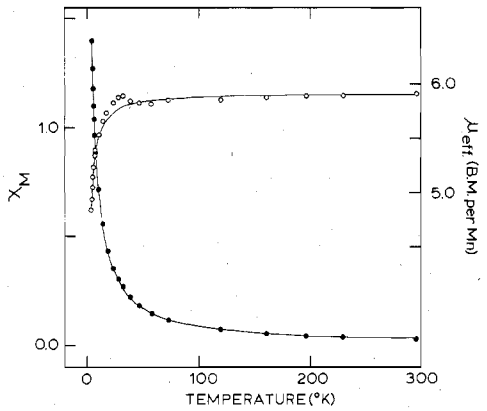

Figure 11. Molar paramagnetic susceptibility (cgsu/mol of dimer) and effective magnetic moment (μ_{eff} in μ_B) per Mn(II) ion vs. temperature curves for $[Mn_2(tren)_2(NCO)_2](BPh_4)_2$.

Mn^{2+} doped into $[Zn(Me_6tren)I]I$. Least-squares fitting the $[Mn_2(tren)_2(NCO)_2](BPh_4)_2$ data to the dimer expressions gave $J = -0.15$ cm^{-1} and $D = -0.29$ cm^{-1} with the assumption that g is isotropic and equal to 2.0. The D value obtained in this case is quite reasonable.

Tables XVI[13] and XVII[13] give the variable-temperature magnetic susceptibility data for $[Mn_2(tren)_2(NCS)_2](BPh_4)_2$ and $[Mn_2(tren)_2(CN)_2](BPh_4)_2$, respectively. The best least-squares fits to the data using theoretical equations both for the $S = {}^5/_2$ monomer and for the $S = S_2 = {}^5/_2$ exchange-interacting dimer are also given in the tables. For the thiocyanate compound, a better fit is obtained using the monomer equations, but, as with the cyanate compound, very unreasonable fitting parameters are obtained ($D = 2.89$ cm^{-1}, $g_\perp = 1.84$, and $g_\parallel = 2.20$). In the case of the fit to the dimer equations, reasonable values of J (−0.13 cm^{-1}) and g (2.00) were obtained, but the D value (−0.001 cm^{-1}) does not seem to be appropriate for this type of compound. The μ_{eff} for $[Mn_2(tren)_2(NCS)_2](BPh_4)_2$ does drop from 5.85 μ_B at 267 K to 5.05 μ_B at 4.2 K, a drop in μ_{eff} which is a little less than observed for the cyanate compound but which certainly exceeds that observed for the monomer. There does seem to be a weak antiferromagnetic exchange interaction present in both the cyanate and thiocyanate compounds.

For $[Mn_2(tren)_2(CN)_2](BPh_4)_2$, μ_{eff} is essentially constant at 6.00 $\mu_B \pm 1\%$ down to 7.9 K, below which there is a decrease. Fitting to the monomer equations gives $g = 2.04$ and $D = 0.60$ cm^{-1}, whereas fitting to the dimer equations gives totally unreasonable parameters. If this compound is indeed dimeric, the magnitude of the exchange interaction must be very small and the possibility that this compound is monomeric cannot be ruled out.

Magnetic susceptibility data were collected for a sample of $[Mn_2(tren)_2Cl_2](BPh_4)_2$, but the presence of significant amounts of impurities, as evidenced by the low (5.64 μ_B) magnetic moment at 296 K, precluded meaningful fitting of the data. Insufficient quantitites of pure $[Mn_2(tren)_2Br_2](BPh_4)_2$ and $[Mn_2(tren)_2(N_3)_2](BPh_4)_2$ could be obtained for susceptibility data collection; however, both of these compounds could be isolated in low yields as crystalline materials.

Since magnetic susceptibility data for $[Mn_2(tren)_2(NCO)_2](BPh_4)_2$ indicated the presence of an antiferromagnetic exchange interaction, several additional EPR experiments were performed in order to understand the complexity of the EPR spectra (see Figures 9 and 10) for this compound. Single crystals of $[Zn_2(tren)_2(NCO)_2](BPh_4)_2$ doped with Mn(II) were prepared. The Q-band EPR spectrum of a powdered sample of these crystals shows two resonances of nearly equal intensity at $g = 3.68$ and $g = 1.94$. Both of these signals are broad, and only the $g = 1.94$ signal shows hyperfine structure. It is possible to distinguish 17 poorly defined hyperfine lines which are spaced at about 90-G intervals. These could be due to Mn(II) pairs in the lattice, a complicated monomer signal, or a poorly doped sample. In any event, the spectrum could not be easily interpreted.

Magnetically dilute samples of $[Mn(Me_6tren)Br](BPh_4)$ and $[Mn_2(tren)_2(NCO)_2](BPh_4)_2$ were also prepared as 77 K glasses using DMF/$CHCl_3$ (1:1) solutions. The X-band glass spectrum of the Me_6tren compound looks similar to the X-band spectrum of Mn-doped $[Zn(Me_6tren)I]I$ except that there are marked differences in relative line widths of the various signals. The Me_6tren glass spectrum is clearly indicative of a monomer with 0.20 cm^{-1} < D < 0.22 cm^{-1}. The X-band glass EPR spectrum of the cyanate compound looked more complicated. It has the appearance of a superposition of a monomer signal similar to that in the Me_6tren glass spectrum and a set of broader features. It was not possible to conclude from the cyanate glass spectrum whether the monomeric $[Mn(tren)(NCO)]^+$ species has zero-field splitting similar to that of the Me_6tren compound. Previous molecular weight studies of $[Cu_2(tren)_2(NCO)_2](BPh_4)_2$ and $[Ni_2(tren)_2(NCO)_2](BPh_4)_2$ did show that there was considerable dissociation of the dimeric cations in solution.

As a final effort to decipher the EPR of $[Mn_2(tren)_2(NCO)_2](BPh_4)_2$, a single-crystal EPR study was undertaken. A crystal was carefully mounted in the Q-band cavity with the crystallographic b axis perpendicular to the direction of the magnetic field. The compound crystallizes in the space group $P2_1/c$ and there are two dimers in the unit cell. In the space group $P2_1/c$, mounting a crystal such that the magnetic field is perpendicular to the b axis gives the only possible orientation of the crystal relative to the magnetic field in which all dimeric cations are magnetically equivalent. The crystal was rotated about the b-axis such that the magnetic field

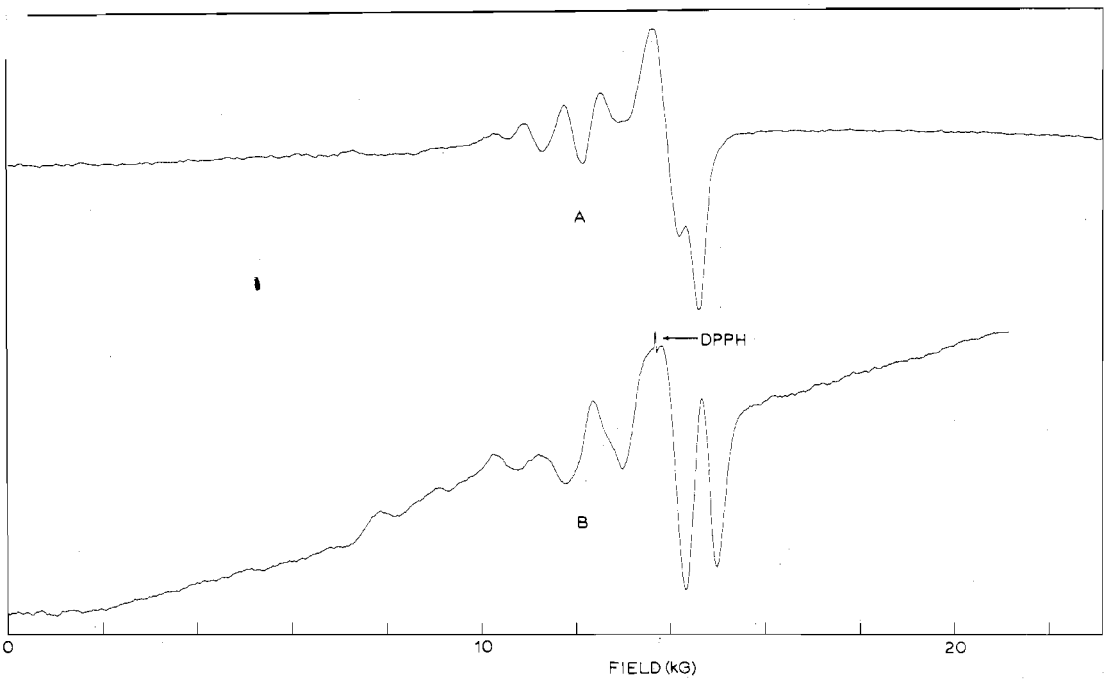

Figure 12. Single-crystal room-temperature Q-band EPR spectra of $[Mn_2(tren)_2(NCO)_2](BPh_4)_2$. The magnetic field is always in the *ac* crystallographic plane. The angular settings are arbitrary: (A) 123° and (B) 33°.

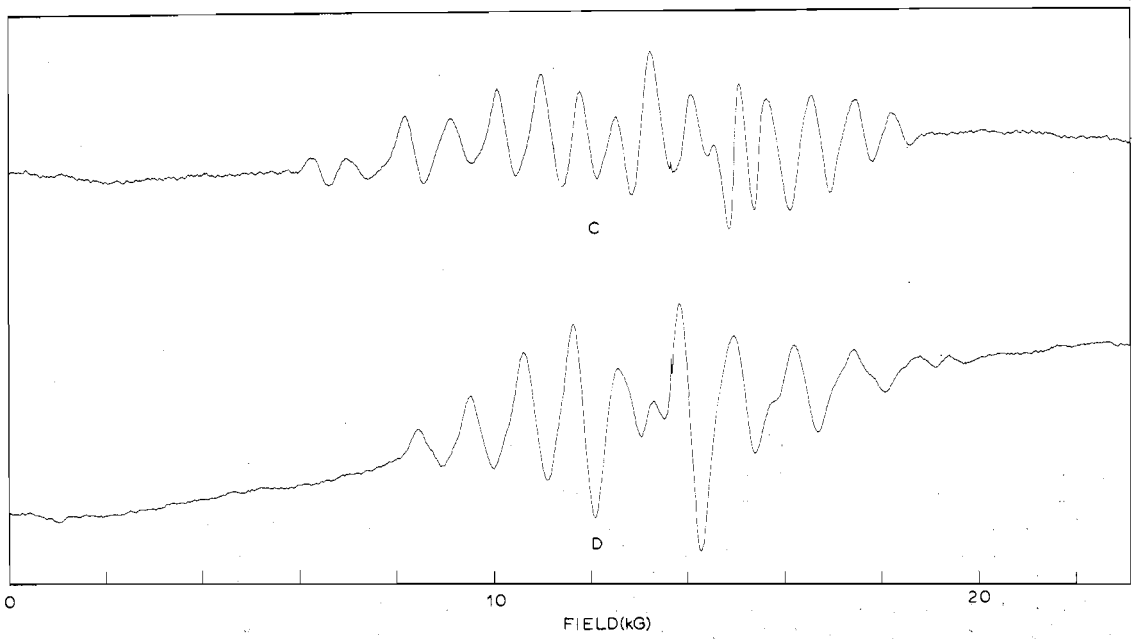

Figure 13. Single-crystal room-temperature Q-band EPR spectra of $[Mn_2(tren)_2(NCO)_2](BPh_4)_2$. The magnetic field is always in the *ac* crystallographic plane. The relative angular settings are (C) 165° and (D) 84°.

moved in the *ac* crystallographic plane, thus maintaining the *b* axis perpendicular to the field. The crystal was observed at 3° intervals over a range of 180°. Figures 12 and 13 show a few of the room-temperature spectra obtained at various crystal settings. Even with the relatively fine grid, it was not possible to trace the angular variation of the various resonances due to the width of peaks and severe overlap problems in the $g = 2$ region. It was obvious, however, that there was a significant angular variation in the spectrum and that at certain angles the spectrum was radically simplified. It should be pointed out that the many features seen in the spectra of Figures 12 and 13 are *not* due to manganese hyperfine interactions but result from single-ion zero-field splittings. The interion zero-field interaction in the cyanate dimer is negligible. If the two Mn(II) ions in a dimer are treated as point dipoles, the interion dipolar interaction can be calculated from the simple expression $D_e = g^2\beta^2/R^3$, where R is the separation between the dipoles. The Mn–Mn distance in the cyanate dimer is 6.0 Å and this gives $D_e = 0.0085$ cm^{-1} (~85 G). Thus, both the manganese hyperfine and interion dipolar effects are concealed in the spectral line widths.

Figure 12 (tracing A) shows the Q-band EPR spectrum obtained at 123°. Using the results of the crystal structure of $[Mn_2(tren)_2(NCO)_2](BPh_4)_2$, it can be calculated that the angle setting of 121.5° corresponds to the position where the manganese–tertiary nitrogen vector is perpendicular to the field. This vector should be close to the magnetic *z* axis of the distorted trigonal bipyramid for each Mn(II) complex and it is interesting that this particular spectrum is the most compressed spectrum in the *ac* plane. In Figure 13, spectra

C and D correspond to the orientations in which the largest and smallest, respectively, effective g values are obtained. As can be seen in Figure 13 considerable features are seen encompassing a range of 14 000 G. At present, it is not possible to give an assignment for the complicated patterns and variations that are seen. As was seen in the discussion of the magnetic susceptibility results, it appears that the relative magnitude of energy splittings due to the electronic Zeeman effect, the single-ion zero-field interaction, and the magnetic exchange interaction for $[Mn_2(tren)_2X_2](BPh_4)_2$ with $X^- = NCO^-$ and NCS^- are all very comparable.

EPR spectra have been assigned for several Mn(II) dimers, but the "dimers" are obtained as pairs of neighboring Mn(II) ions doped into a diamagnetic host lattice.[30] In these doped samples, of course, there is present a large number of isolated (i.e., monomeric) Mn(II) ions. Also, it is not possible to know the exact dimensions and magnetic exchange characteristics of the doped ion pairs. The compound $[Mn_2(tren)_2(NCO)_2](BPh_4)_2$ almost serves the purpose of providing a pure compound with a resolved EPR spectrum. The large BPh_4^- ions come close to affording an effective degree of magnetic dilution for the outer-sphere dimers. Perhaps a slightly larger anion or lower sample temperatures for the single-crystal study will give a spectral resolution improved to the point where the various spectral features can be assigned.

Acknowledgment. We are very grateful for support from National Institutes of Health Grant HL13652 and for funds for computing from the University of Illinois Research Board.

Appendix

In the calculations for an exchange-interacting manganese(II) dimer, it was assumed that the magnetic exchange interaction is isotropic and there is no rhombic single-ion zero-field splitting. It is convenient to work in a coupled basis set where the total spin S is given as $S = S_1 + S_2$. The spin Hamiltonian operator is

$$\hat{H} = g_{\parallel}\beta\hat{H}_z\cdot\hat{S}_z + g_{\perp}\beta(\hat{H}_x\cdot\hat{S}_x + \hat{H}_y\cdot\hat{S}_y) + D[\hat{S}_z^2 - {}^1/_3S(S+1)] - 2J\hat{S}_1\cdot\hat{S}_2$$

A coupled basis set, $|S, M_s\rangle$, is used for the wave functions. These can be obtained with Wigner coefficients, and for the manganese(II) dimer, where $S_1 = S_2 = {}^5/_2$, they are tabulated by Owen and Harris in ref 30. With these coupled wavefunctions and the Hamiltonian operator given above, the Hamiltonian energy matrix can be constructed readily. The following upper-right-triangle nonzero matrix elements are obtained:

$\langle 5, \pm5|\mathcal{H}|5, \pm5\rangle = -30J + 25D/2 \pm 5g_z\beta H_z$

$\langle 5, \pm4|\mathcal{H}|5, \pm4\rangle = -30J + 17D/2 \pm 4g_z\beta H_z$

$\langle 5, \pm3|\mathcal{H}|5, \pm3\rangle = -30J + 97D/18 \pm 3g_z\beta H_z$

$\langle 5, \pm2|\mathcal{H}|5, \pm2\rangle = -30J + 19D/6 \pm 2g_z\beta H_z$

$\langle 5, \pm1|\mathcal{H}|5, \pm1\rangle = -30J + 11D/6 \pm g_z\beta H_z$

$\langle 5, 0|\mathcal{H}|5, 0\rangle = -30J + 25D/18$

$\langle 4, \pm4|\mathcal{H}|4, \pm4\rangle = -20J + 17D/2 \pm 4g_z\beta H_z$

$\langle 4, \pm3|\mathcal{H}|4, \pm3\rangle = -20J + 13D/2 \pm 3g_z\beta H_z$

$\langle 4, \pm2|\mathcal{H}|4, \pm2\rangle = -20J + 71D/14 \pm 2g_z\beta H_z$

$\langle 4, \pm1|\mathcal{H}|4, \pm1\rangle = -20J + 59D/14 \pm g_z\beta H_z$

$\langle 4, 0|\mathcal{H}|4, 0\rangle = -20J + 55D/14$

$\langle 3, \pm3|\mathcal{H}|3, \pm3\rangle = -12J + 101D/18 \pm 3g_z\beta H_z$

$\langle 3, \pm2|\mathcal{H}|3, \pm2\rangle = -12J + 35D/6 \pm 2g_z\beta H_z$

$\langle 3, \pm1|\mathcal{H}|3, \pm1\rangle = -12J + 179D/30 \pm g_z\beta H_z$

$\langle 3, 0|\mathcal{H}|3, 0\rangle = -12J + 541D/90$

$\langle 2, \pm2|\mathcal{H}|2, \pm2\rangle = -6J + 55D/14 \pm 2g_z\beta H_z$

$\langle 2, \pm1|\mathcal{H}|2, \pm1\rangle = -6J + 95D/14 \pm g_z\beta H_z$

$\langle 2, 0|\mathcal{H}|2, 0\rangle = -6J + 325D/14$

$\langle 1, \pm1|\mathcal{H}|1, \pm1\rangle = -2J + 37D/10 \pm g_z\beta H_z$

$\langle 1, 0|\mathcal{H}|1, 0\rangle = -2J + 101D/10$

$\langle 0, 0|\mathcal{H}|0, 0\rangle = 35D/6$

$\langle 5, \pm3|\mathcal{H}|3, \pm3\rangle = (80/81)^{1/2}D$

$\langle 5, \pm2|\mathcal{H}|3, \pm3\rangle = (20/9)^{1/2}D$

$\langle 5, \pm1|\mathcal{H}|3, \pm1\rangle = (400/126)^{1/2}D$

$\langle 5, 0|\mathcal{H}|3, 0\rangle = (2000/567)^{1/2}D$

$\langle 4, \pm2|\mathcal{H}|2, \pm2\rangle = -(180/49)^{1/2}D$

$\langle 4, \pm1|\mathcal{H}|2, \pm1\rangle = -(720/98)^{1/2}D$

$\langle 4, 0|\mathcal{H}|2, 0\rangle = -(3/98)^{1/2}D$

$\langle 3, \pm1|\mathcal{H}|1, \pm1\rangle = -(12/175)^{1/2}D$

$\langle 3, 0|\mathcal{H}|1, 0\rangle = -(2592/175)^{1/2}D$

$\langle 2, 0|\mathcal{H}|0, 0\rangle = (896/9)^{1/2}D$

$\langle 5, 5|\mathcal{H}_x|5, 4\rangle = (10/4)^{1/2}g_x\beta H_x$

$\langle 5, 4|\mathcal{H}_x|5, 3\rangle = (18/4)^{1/2}g_x\beta H_x$

$\langle 5, 3|\mathcal{H}_x|5, 2\rangle = 6^{1/2}g_x\beta H_x$

$\langle 5, 2|\mathcal{H}_x|5, 1\rangle = 7^{1/2}g_x\beta H_x$

$\langle 5, 1|\mathcal{H}_x|5, 0\rangle = (30/4)^{1/2}g_x\beta H_x$

$\langle 5, 0|\mathcal{H}_x|5, -1\rangle = (30/4)^{1/2}g_x\beta H_x$

$\langle 5, -1|\mathcal{H}_x|5, -2\rangle = 7^{1/2}g_x\beta H_x$

$\langle 5, -2|\mathcal{H}_x|5, -3\rangle = 6^{1/2}g_x\beta H_x$

$\langle 5, -3|\mathcal{H}_x|5, -4\rangle = (18/4)^{1/2}g_x\beta H_x$

$\langle 5, -4|\mathcal{H}_x|5, -5\rangle = (10/4)^{1/2}g_x\beta H_x$

$\langle 4, 4|\mathcal{H}_x|4, 3\rangle = 2^{1/2}g_x\beta H_x$

$\langle 4, 3|\mathcal{H}_x|4, 2\rangle = (14/4)^{1/2}g_x\beta H_x$

$\langle 4, 2|\mathcal{H}_x|4, 1\rangle = (18/4)^{1/2}g_x\beta H_x$

$\langle 4, 1|\mathcal{H}_x|4, 0\rangle = 5^{1/2}g_x\beta H_x$

$\langle 4, 0|\mathcal{H}_x|4, -1\rangle = 5^{1/2}g_x\beta H_x$

$\langle 4, -1|\mathcal{H}_x|4, -2\rangle = (18/4)^{1/2}g_x\beta H_x$

$\langle 4, -2|\mathcal{H}_x|4, -3\rangle = (14/4)^{1/2}g_x\beta H_x$

$\langle 4, -3|\mathcal{H}_x|4, -4\rangle = 2^{1/2}g_x\beta H_x$

$\langle 3, 3|\mathcal{H}_x|3, 2\rangle = (6/4)^{1/2}g_x\beta H_x$

$\langle 3, 2|\mathcal{H}_x|3, 1\rangle = (10/4)^{1/2}g_x\beta H_x$

$\langle 3, 1|\mathcal{H}_x|3, 0\rangle = 3^{1/2}g_x\beta H_x$

$\langle 3, 0|\mathcal{H}_x|3, -1\rangle = 3^{1/2}g_x\beta H_x$

$\langle 3, -1|\mathcal{H}_x|3, -2\rangle = (10/4)^{1/2}g_x\beta H_x$

$\langle 3, -2|\mathcal{H}_x|3, -3\rangle = (6/4)^{1/2}g_x\beta H_x$

$$\langle 2, 2|\mathcal{H}_x|2, 1\rangle = g_x\beta H_x$$

$$\langle 2, 1|\mathcal{H}_x|2, 0\rangle = (6/4)^{1/2}g_x\beta H_x$$

$$\langle 2, 0|\mathcal{H}_x|2, -1\rangle = (6/4)^{1/2}g_x\beta H_x$$

$$\langle 2, -1|\mathcal{H}_x|2, -2\rangle = g_x\beta H_x$$

$$\langle 1, 1|\mathcal{H}_x|1, 0\rangle = 2^{-1/2}g_x\beta H_x$$

$$\langle 1, 0|\mathcal{H}_x|1, -1\rangle = 2^{-1/2}g_x\beta H_x$$

Diagonalization of this energy matrix, then, gives the energies of the six $S_1 = S_2 = {}^5/_2$ dimer states for given values of the magnetic field H, the single-ion zero-field splitting parameter D and $g_\perp$ ($= g_x = g_y$) and $g_\parallel$. The magnetic susceptibilities were measured at 12.0 kG and the magnetic moment μ_i of the ith dimer state is evaluated as the partial derivative (i.e., "slope" or change) of the energy E_i of the ith dimer state as a function of the magnetic field determined at 12.0 kG.

$$\mu_i = -\partial E_i/\partial H$$

The magnetic moments of the various dimer states are each weighted in a Boltzmann distribution to give the molar paramagnetic susceptibility (χ_M) as

$$\chi_M = \frac{N}{H}\frac{\sum_i -\mu_i \exp(-E_i/kT)}{\sum_i \exp(-E_i/kT)}$$

The diagonalization and χ_M evaluation were coupled to a function-minimization procedure to least-squares-fit the data. Thus, in each cycle of the fitting the Hamiltonian matrix is set up with J, D, $g_\parallel$, and $g_\perp$ and then diagonalized to give χ_M.

The spin Hamiltonian for a d^5 monomer was taken as

$$\hat{H} = g_\parallel\beta\hat{H}_z\cdot\hat{S}_z + g_\perp\beta(\hat{H}_x\cdot\hat{S}_x + \hat{H}_y\cdot\hat{S}_y) + D[\hat{S}_z^2 - {}^1/_3S(S+1)]$$

Hamiltonian matrix elements were derived as above using the appropriate spin functions. The matrix was diagonalized to give the energies of each of the six eigenfunctions for given values of the magnetic field H, the axial zero-field splitting parameter D, and $g_\parallel$ and $g_\perp$. The molar paramagnetic susceptibility was evaluated as was done in the dimer case. Again, a function-minimization routine was used with the matrix diagonalization in a least-squares fitting procedure.

Registry No. $[Mn_2(tren)_2(NCO)_2](BPh_4)_2$, 64682-56-0; $[Mn_2(tren)_2(NCS)_2](BPh_4)_2$, 64682-58-2; $[Mn_2(tren)_2(C_2O_4)](BPh_4)_2$, 64871-86-9; $[Mn_2(tren)_2(N_3)_2](BPh_4)_2$, 64682-60-6; $[Mn_2(tren)_2(CN)_2](BPh_4)_2$, 64682-62-8; $[Mn_2(tren)_2Cl_2](BPh_4)_2$, 64682-64-0; $[Mn_2(tren)_2Br_2](BPh_4)_2$, 64682-66-2; $[Mn(Me_6tren)Br]Br$, 55684-66-7; $[Mn(Me_6tren)I]I$, 13964-85-7; $[Zn(Me_6tren)I]I$, 13964-87-9.

Supplementary Material Available: Final $|F_o|$ and $|F_c|$ values for $[Mn_2(tren)_2(NCS)_2](BPh_4)_2$ and $[Mn_2(tren)_2(NCO)_2](BPh_4)_2$, and Tables I (analytical data), XI and XII (results of least-squares planes calculations for the BPh_4^- phenyl groups in the cyanate and thiocyanate compounds), and XIV–XVII (observed and theoretically calculated variable-temperature magnetic susceptibility data for $[Mn(Me_6tren)Br]Br$, $[Mn_x(tren)_x(NCO)_x](BPh_4)_x$, $[Mn_x(tren)_x(NCS)_x](BPh_4)_x$, and $[Mn_x(tren)_x(CN)_x](BPh_4)_x$ (x = 1 or 2), respectively) (48 pages). Ordering information is given on any current masthead page.

References and Notes

(1) Part 12: T. R. Felthouse and D. N. Hendrickson, *Inorg. Chem.*, preceding paper in this issue.
(2) Camille and Henry Dreyfus Fellow, 1972–1977; A. P. Sloan Foundation Fellow, 1976–1978.
(3) E. J. Laskowski, D. M. Duggan, and D. N. Hendrickson, *Inorg. Chem.*, **14**, 2449 (1975).
(4) D. N. Hendrickson and D. M. Duggan, *ACS Symp. Ser.*, **No. 5** (1974).
(5) D. M. Duggan and D. N. Hendrickson, *Inorg. Chem.*, **13**, 2929 (1974).
(6) R. Y. Yanagida, T. B. Vance, Jr., and K. Seff, *J. Chem. Soc., Chem. Commun.*, 382 (1973).
(7) C. Pelizzi and G. Pelizzi, *Acta Crystallogr., Sect. B*, **30**, 2421 (1974).
(8) F. L. Phillips, F. M. Shreeve, and A. C. Skapski, *Acta Crystallogr., Sect. B*, **32**, 687 (1976).
(9) B. Gonzalez, J. Kouba, S. Yee, C. A. Reed, J. F. Kirner, and W. R. Scheidt, *J. Am. Chem. Soc.*, **97**, 3247 (1975).
(10) G. Ciani, M. Manassero, and M. Sansoni, *J. Inorg. Nucl. Chem.*, **34**, 1970 (1972).
(11) M. DiVaira and P. L. Orioli, *Acta Crystallogr., Sect. B*, **24**, 1269 (1968).
(12) E. Sinn, *J. Chem. Soc., Dalton Trans.*, 162 (1976).
(13) Supplementary material.
(14) Computer programs used include ALF (Fourier synthesis), ORFLS (least-squares data refinement by Busing and Levy), JAM (distances and angles with esd's), BESTP (least-squares planes by M. E. Pippy), HYGEN (hydrogen atom generation by F. K. Ross), and ORTEP (thermal ellipsoid drawings by C. K. Johnson).
(15) H. P. Hansen, E. Herman, J. D. Lea, and S. Skillman, *Acta Crystallogr.*, **17**, 1040 (1964).
(16) D. T. Cromer and J. B. Mann, *Acta Crystallogr., Sect. A*, **24**, 321 (1968).
(17) "International Tables for X-ray Crystallography", Vol. III, Kynoch Press, Birmingham, England, 1962.
(18) "International Tables for X-ray Crystallography", Vol. IV, Kynoch Press, Birmingham, England, in press.
(19) D. M. Duggan and D. N. Hendrickson, *Inorg. Chem.*, **13**, 1911 (1974).
(20) R. J. Sime, R. P. Dodge, A. Zalkin, and H. D. Templeton, *Inorg. Chem.*, **10**, 537 (1971).
(21) E. J. Laskowski, Ph.D. Thesis, University of Illinois, 1976.
(22) R. D. Dowsing, J. F. Gibson, D. M. L. Goodgame, M. Goodgame, and P. J. Hayward, *Nature (London)*, **219** 1037 (1968).
(23) R. D. Dowsing, J. F. Gibson, M. Goodgame, and P. J. Hayward, *J. Chem. Soc. A*, 187 (1969).
(24) D. M. L. Goodgame, M. Goodgame, and P. J. Hayward, *J. Chem. Soc. A*, 1352 (1970).
(25) R. D. Dowsing and J. F. Gibson, *J. Chem. Phys.*, **50**, 294 (1969).
(26) E. A. Harris, *J. Phys. C*, **5**, 338 (1972).
(27) G. L. McPherson and J. R. Chang, *Inorg. Chem.*, **15**, 1018 (1976).
(28) F. Chiarini, M. Maatinelli, and G. Ranieri, *J. Magn. Reson.*, **14**, 60 (1974).
(29) W. C. Tennant, *J. Magn. Reson.*, **14**, 152 (1974).
(30) J. Owen and E. A. Harris in "Electron Paramagnetic Resonance", S. Geschwind, Ed., Plenum Press, New York, N.Y., 1974, Chapter 6.